PALEOENVIRONMENTAL RECONSTRUCTION OF PALEOLAKE MABABE, NORTHWESTERN BOTSWANA FROM SEDIMENT CHEMISTRY AND BIOLOGICAL PRODUCTIVITY DATA

By

KRISTI L. TETER

Bachelor's of Science in Geology

Oklahoma State University

Stillwater, OK

2007

Submitted to the Faculty of the
Graduate College of the
Oklahoma State University
in partial fulfillment of
the requirements for
the Degree of
MASTER OF SCIENCE
December, 2009

PALEOENVIRONMENTAL RECONSTRUCTION OF PALEOLAKE MABABE, NORTHWESTERN BOTSWANA FROM SEDIMENT CHEMISTRY AND BIOLOGICAL PRODUCTIVITY DATA

Thesis Approved:

Dr. Eliot Atekwana

Thesis Adviser

Dr. Anna Cruse

Dr. Estella Atekwana

Dr. Carlos Cordova

Dr. A. Gordon Emslie

Dean of the Graduate College

ACKNOWLEDGMENTS

I wish to first thank the members of my thesis committee who provided knowledge and understanding through the process. I would like to acknowledge my thesis advisor Dr. Eliot Atekwana. Dr. Atekwana has provided an immense about of guidance over the past few years and always demonstrated a great desire to assist in the furthering of my research and my understanding of the Mababe Depression. He also provided comic relief along the way. Dr. Anna Cruse assisted wonderfully with editing, laboratory analysis, and data interpretation, while providing moral support and encouragement. Dr. Estella Atekwana helped to broaden my understanding of the region and geology at play. Dr. Estella Atekwana also made the project possible and put in a great amount of time and energy to make the research trips to Botswana possible. These were truly great experiences that will have a lasting impression on my future. Dr. Carlos Cordova exhibited great patience and understanding while also providing a much needed outside prospective. Dr. Cordova provided much need encouragement and positive reinforcement. I greatly thank each member of my committee because without their support I would not have been able to achieve this feat.

I acknowledge support from the National Science Foundation to conduct this International Research Experience for Students (IRES). The IRES grant gave me tremendous experience working in an international setting and that is a great resource to my future career.

The University of Botswana and the Harry Oppenheimer Okavango Research Center were both instrumental in my ability to conduct this research in Botswana. I would like to acknowledge Dr. Motsoptse Modisi, Dr. Elisha Shemang, and Dr. Loago Molwalefhe from the University of Botswana for their role in organizing the field research, assisting in the field work, and for being wonderful hosts while I was in Botswana. I would like to thank Dr. Susan Ringrose, Dr. Phillipa Huntsman-Mapilla, and Thebe from the Harry Oppenheimer Okavango Research Center for assisting with the field sediment sampling. Although not mentioned by name the people of the Mababe Village deserve my gratitude for generously extending their hospitality. I would also like to thank Kelsey Mosely, Andy Foreman, and Cody Winchester for the assistance in the field and for helping to make each of the trips memorable and fun. Jennifer Gamrod is appreciated for her contributions to the research. She was instrumental in its overall success.

Jennifer Latimer from Indiana State University deserves a special thanks for the intellectual knowledge she provided and for the analysis of the phosphorus in the sediments.

Lastly, I thank my friends and family for their support over the last few years. My parents provided the encouragement and financial support necessary to complete my degree. Andrea and Steven were always patient listeners when I needed to talk to someone. My family often let my needs come first while I was working on this thesis and will always be greatly appreciated. My friends were a wonderful break and distraction from work but also contributed greatly to the process by assisting in the laboratory, helping with computer difficulties and frustrations, and providing great intellectual input. I have made some wonderful friendships in the last few years and will always love the memories I have from graduate school of the trips we took and evenings we spent together. I give a special thanks to Courteney Baker, Jessica Magers, Annie Drewry, Jason Faith, and Tyler Treece for listening and supporting me when I became unreasonable.

TABLE OF CONTENTS

Chapter Page

LIST OF FIGURES

Figure Page

CHAPTER I

INTRODUCTION

The Mababe Depression is located in northern Botswana on the northeast distal end of the Okavango Delta (Fig. 1). While the region is currently arid, and the Mababe Depression is dry, geological evidence such as beach ridges and thick accumulations of lacustrine deposits indicate that the Mababe Depression once contained a large lake (Grove, 1969; Cooke, 1979). Past research aimed to understand why the landscape of northern Botswana is dominated by low relief aeolian, fluvial, and lacustrine landforms related to the Okavango Delta and a large paleolake system (Grey and Cooke, 1977; Shaw, 1985). Beach ridges are found at discrete elevations (945 m and 936 m above sea level (asl)) in and around the Mababe Depression, providing direct evidence for cycles of static lake levels at those elevations. Two similar geomorphic features in Lake Ngami and the Makgadikgadi Pans, are believed to be part of the same paleolake system. These features have corresponding beach ridges along their northwestern edge at elevations equivalent to the ridges found in the Mababe Depression (Shaw, 1997).

At present, water flow into the Mababe Depression occurs intermittently via the Mababe and Savuti channels (Burrough and Thomas, 2008) which enter the depression and form the Mababe and Savuti swamps (Fig. 2). In the past, the Guatumbi and Ngwezumba Rivers (Fig. 2) have contributed inflow to the basin along its eastern edge. Currently, northern Botswana receives most of its surface water as riverine input from the tropics, specifically the highland areas of central Angola, but past periods of increased local precipitation may have directly influenced the spatial extent of the lake occupying the Mababe Depression (e.g., Burrough and Thomas, 2008). The internal paleo-hydrodynamic processes of Lake Paleo-Mababe must be resolved to better understand the physical controls that influenced the dramatic shifts in the surface-hydrology of northern Botswana.

Previous geomorphic and chronological studies of the Mababe Depression have focused on the interpretation of preserved beach ridges (Du Toit, 1926; Grove, 1969; Cooke and Verstappen, 1984; Shaw, 1985; Burrough et al., 2007; Burrough and Thomas, 2008). The early work on the geomorphology of the region has provided evidence that the hydrology of the region has drastically changed. These changes primarily include the dessication of large lakes and the disappearance and alteration of fluvial systems (Cooke and Verstappen, 1984). Recent studies based on the chronology of the beach ridges use ^{14}C, thermoluminescence (TL), and optically stimulated luminescence (OSL) dating techniques to constrain temporal changes that occurred to the elevation and extent of the lakes in northwestern Botswana (Shaw, 1985; Burrough and Thomas, 2008). These chronologies from the beach ridges date periods of ridge building through wave action and therefore are a discontinuous record of the lake history and do not provide a complete understanding of processes that occurred between these different high water events (Burrough and Thomas, 2008).

The present research hypothesizes that biological productivity data in the sediment record of the Mababe Depression records changes in the hydrology driven by climate and/or tectonics. Sediments collected from the paleolake basin provide a sedimentary record and the opportunity to reconstruct the paleo-chemistry, and the lacustrine and terrestrial paleo-productivity associated with responses to temporal variations in the overall water balance. This involves employing several biogeochemical proxies, such as sediment leach chemistry, carbon, phosphorus and biogenic silica concentrations and the stable carbon isotopic compositions of the organic matter, to elucidate changes in lake water chemistry and biological productivity, and ultimately, infer the mechanisms responsible for those changes. The sediments were sampled from a 560 cm-deep trench in the southeast Mababe Depression (Fig. 2). The sediment leach chemistry provides information on the salinity and solute fraction of water in the lake that induced precipitation in the sediments. The phosphorus speciation data is used to understand erosion in the watershed, as well as nutrient availability for productivity of plankton in the lake. Changes in biological productivity are determined using biogenic silica, total organic carbon concentrations (C_{org}), carbon-to-nitrogen ratios (C:N), and the stable carbon isotopic composition of organic carbon ($\delta^{13}C_{org}$). Studies in Lake Ngami by Huntsmann-Mapilla et al. (2006) have demonstrated that changes in sediment chemistry provide information on changing chemical conditions that in turn, affect biological productivity in lacustrine settings. Inferences can be made from biological productivity and sediment chemistry about the processes influencing the lake i.e., climate

change and tectonic effects. Optically stimulated luminescence dates of several horizons are used to place the history of Paleolake Mababe within a regional context, and to further explore the relative importance of climate versus tectonic processes on the stability of a lacustrine system.

This study provides information on how the environment and hydrologic regime responded to changes in the climate and lithospheric/surface interactions. Historical environmental response is a key to understanding how future changes in the environment will affect the hydrology in northwestern Botswana. The study relates to the natural response of climate change and may prove to be valuable when trying to evaluate anthropogenic influences to the regions climate and the associated environmental response (e.g., Andersson et al., 2006). An understanding of the environmental sensitivity to anthropogenic changes will influence decisions in the water management of the Okavango Delta especially in regards to responsibly addressing the growing strain on the region's water supply due to population growth (e.g., Kgathi et al., 2006).

CHAPTER 2

STUDY SITE

The Mababe Depression serves a unique setting for an investigation of paleolacustrine environmental history in northern Botswana. The Depression is located in a region characterized by a complex set of landforms from both arid (dunes, salt pans, and deposits of calcretes and silcretes) and humid (beach ridges, swamplands, lake strandlines and beds) environments (Grey and Cooke 1977). Evidence suggests that lacustrine conditions were present in the Depression from early as the late Pleistocene and extend through most of the Holocene (Grey and Cooke, 1977; Burrough and Thomas, 2008; Burrough and Thomas, 2009). This paleolake is unique in that it existed in a region that has experienced a largely arid climate, and thus is particularly sensitive to water budget fluctuations. Water budget changes can be caused by both local climate changes (e.g., changes in precipitation and/or evaporation rates) and distal events in the African tropics, where the headwaters of the Okavango River are located. Additionally, Paleolake Mababe has also been affected by tectonic events (Gamrod, 2009; Ringrose et al., 2005). Studies indicate that the Savuti River is an underfit channel because in the past large quantities of water entered the Mababe Depression via the Savuti from the Kwando River that has been diverted away from the depression due to tectonic activity (Shaw, 1988; Gamrod, 2009). The changes in local and distal climate and regional tectonics are reflected in the biogeochemical proxies, as the ecosystem responded to variations in lake chemistry and water depth.

2.1. Mababe Depression morphology

The Mababe Depression is a heart-shaped, 3,000 km^2 depression in northern Botswana, located east of the Okavango Delta between 18° and 19°

30’ S and 24°and 24°30’ E (Shaw, 1985; Fig. 2). The Depression is a terminus for the Okavango drainage system, along with Lake Ngami and the Makgadikgadi Pans.

The Mababe Depression is bounded on the west by the Magikwe Ridge, a large complex of beach ridges extending 75 km from the Mababe River in the south to the Goha Hills in the north (Fig. 2). Beach ridges form during a standstill in lake levels, when sediments begin to aggrade at the stabilized elevation thresholds (DeVogel et al., 2004; Burrough and Thomas, 2008). The beach ridges in the Mababe Depression indicate stable lake levels persisted at 945 m and 936 m asl. The Magikwe Ridge consists of one or two ridges at an elevation of 940-945 m asl, but at the southern end of the Magikwe Ridge and between the Goha Hills and the Savuti River, a parallel ridge was formed at 936 m asl (Shaw, 1985). The Magikwe Ridge is tilted to the south as a result of tectonic activity post ridge formation (Burrough and Thomas, 2008). The 936 m asl beach ridge also is apparent in the eastern portion of the Mababe Depression paralleling the escarpment from the Mababe River to the Gautumbi delta, and again appearing as two ridges at the mouth of the Ngwezumba River (Burrough and Thomas, 2008).

In the Mababe Depression, other features such as strandlines and river terraces also correspond to elevations of stable water levels. The 930 m asl is the most widespread of these elevation thresholds with terraces located both in the Mababe and Savuti Rivers and strandlines at the Ngwezumba and Ghautumbi deltas. The Mababe Depression sump level is clearly defined at 919-923 m asl by a change in the vegetation from Mopane scrub to Acacia dominated parkland (Shaw, 1985).

The beach ridges and strandlines in the Mababe Depression can be traced to other geomophological similar features including Lake Ngami and the Makgadikgadi Pans. These remnant beaches of the Mababe Depression are correlated to ridges found in Lake Ngami, the Makgadikgadi Pans, and the Lake Caprivi and indicate the presence of an extensive paleo-lacustrine system that dominated the past landscape. The presence of such a large lake up to 120,000 km^2 (Shaw, 1988) in this now arid environment requires drastic changes in the water balance. The change from an environment that supported the once extensive lake system to the current arid environment could have been driven by climatic variations (e.g., decreased precipitation) or changes in the fluvial systems draining into the region.

2.2. Hydrology and climate of the Mababe Depression

The Mababe Depression is located in the middle Kalahari Desert, and at present, this region is a semi-arid environment (Passarge, 1904 in Shaw, 1985). Northern Botswana is located in the southern African Summer Rainfall Zone and is influenced by both the position of the Inter-Tropical Convergence Zone (ITZC) and by anti-cyclonic conditions in southern Africa (Huntsmann- Mapila et al., 2006; Burrough et al., 2007). The average annual precipitation is about 500 mm/yr (McCarthy et al., 2000), while the mean average evaporation rate of 2200 mm/yr exceeds the rate of precipitation (McCarthy et al., 1998).

The inflow into northern Botswana is controlled by local precipitation and runoff from the Angolan tropical catchment. A significant portion of the inflow in northern Botswana is derived from the rivers flowing from the tropical highlands of Angola via the Okavango and Kwando River systems (Fig. 1). Inflow from the tropical catchment is dependent upon the position of the ITZC and the Congo Air Boundary (CAB) (Huntsmann- Mapila et al., 2006). The river inflow from the Angolan highlands is out of phase with local precipitation that falls mainly between November and March (Shaw, 1986). Four rivers have contributed water to the Mababe Depression throughout the late Pleistocene and Holocene: the Mababe, Savuti, Ngwezumba, and Gautumbi (Fig. 2). The Mababe River is a confluence of the Thamalakane and Kwai Rivers that flow east from the Okavango Delta. The Savuti River flows east from the Kwando River into the Linyanti swamp, before flowing southeast into the Mababe Depression. The Ngwezumba and Gautumbi Rivers delivered water to the Mababe Depression from catchments to the east that drain the area along the Botswana-Zimbabwe border (Shaw, 1986). Water that flows into the Mababe Depression from the Angolan highlands along the rivers pass through either the Okavango Delta located to the west of the Mababe Depression or through the Linyanti swamp to the north of the Depression. Both the Okavango Delta and the Linyanti swamp are wetland environments that contrast the surrounding semi-arid Kalahari. The majority of the water that enters the Okavango Delta and Linyanti swamp is lost to evapo-transpiration because the Okavango and Kwando Rivers slow and spread laterally after entering the low lying Okavango graben. Only 2% of the 15 km^3 of water that enters the Okavango Delta each year exits as surface flow (McCarthy et al., 1988). The interaction of the semi-arid desert and the wetland environments of the Okavango Delta and Linyanti swamp make the study area unique. The endoreic Okavango River and the Kwando River have resulted in a network of wetland conditions that extend to the Mababe Depression where the Mababe and Savuti swamps remain active despite the seasonal nature of hydrological input and high evapo-transpiration rates.

The Mababe Depression has not continuously contained water during the past 200 years that written records have been kept (Shaw, 1986). However, oral tradition indicates that a lake existed during the 18th century (Shaw, 1986). Water has not been historically recorded in the Gautumbi River, but the Mababe, Savuti, and Ngwezumba all have been recorded to flow in the last 200 yrs into the Depression, during years of record flooding (Shaw, 1985). It has also been noted by Shaw (1985) that the Thamalakane River that contributes to the Mababe River can flow both into and away from the Mababe Depression due to the low relief of the region.

2.3 Geology of northwestern Botswana

The Mababe Depression is situated in the Okavango Rift Zone (ORZ). The ORZ is a half-graben structure bound by normal faults with downthrow of up to 300 m (Modisi et al. 2000). The ORZ is a seismically active rift trending NE-SW and is bounded by the Gomare, Kunyare, and Thamalakane faults (Milzow et al., 2009). Tectonics along the ORZ caused uplift of the Zimbabwe-Kalahari axis during the late Pliocene and resulted in the impoundment of the proto Okavango, Kwando, and upper Zambezi drainage and the development of the Mababe, Ngami, and Makgadikgadi subbasins (Haddon and McCarthy, 2005; Ringrose, 2005).

The surficial geology of northern Botswana is dominated by a thick accumulation of Cenozoic sands and silts that compose the Kalahari beds (Thomas and Shaw, 1991; Milzow et al., 2009). The thickness of the Kalahari bed sediments can be up to 300 m thick in areas around the faults (Shaw, 1985; Milzow et al., 2009). Duricrust formation is found associated with the deltaic and aeolian sands and silts of the Kalahari beds (Milzow et al., 2009). Calcrete-silcrete integrade duricrusts are common to the Kalahari environment and occur both at the subsurface from groundwater saturation and at the surface as a result of evapotranspiration (McCarthy and Ellery, 1995; Kampunzu et al., 2007).

CHAPTER 3

METHODOLOGY

3.1 Sediment sampling

Lake sediments were sampled in the southeast portion of the Mababe Depression near the terminus of the Mababe River in June 2007 (Fig. 2). A trench was excavated at location MABX (E 24°05' 04.8", S 19°06' 19.8"). The depth of trench MABX was 560 cm. Samples were collected at 5 cm intervals except at 545 cm and 555 cm due to difficulty of sampling. Samples were placed in labeled sample bags and transported back to the laboratory for further analyses. While in the field the sediments on the trench face were described on the basis of their color, grain size and observed mineralogical content. Back in the laboratory Munsel color descriptions were assigned to dried samples.

Boulder sized samples were taken from the trenche for optically stimulated luminescence (OSL) dating in the MABX trench at the depths of 45, 135, 380, and 500 cm. These samples were retrieved from the trench face from sediments that were well consolidated to ensure that the core of the sample was not exposed to light. The samples were then wrapped in aluminum foil and taped for transportation to the laboratory.

3.2 Sample analyses

3.2.1 Dry bulk density

The dry bulk density was determined by gravimetric analysis. Containers with known volume were filled with sediment samples that had been air dried. The sediment was packed in the pre-weighed containers by tapping the exterior of the container. The sediment mass was determined. The mass was then divided by the known volume of the container to estimate the dry bulk density.

3.2.2 Sediment leaching

Sediments were leached with deionised water and the electrical conductivity, pH, and major cations and anions were measured from the solution. A portion of the sample was removed from the plastic storage bag and crushed using a mortar and pestle. Approximately 100 mg of sample was weighed and placed in a 50 ml centrifuge tube. Fifty ml of deionised water (18 ΩOhm) was dispensed into each centrifuge tube using a repipetter. The samples were allowed to leach for 24 hours while being continuously shaken by a mechanical shaker. After 24 hours, the samples were centrifuged for 10 minutes at 4000 rpm. A 10 ml aliquot of the liquid sample was poured into a 15 ml centrifuge tube. The rest of the liquid was used to measure the electrical conductivity using a conductivity meter (Fisher Scientific) and pH using a pH meter (Metler Toledo). The conductivity and pH meters were calibrated using standards according to the manufacturer's instructions. The alkalinity was determined by acid titration (Hach, 1993). The 10 ml aliquot samples were used to measure anions (Cl, SO_4, NO_3) and cations (K, Na, Ca, Mg) by a Dionex ICS 3000 ion chromatography.

3.2.3 Biogenic silica

Biogenic silica was analyzed following the molybdate-blue spectrophotometry method outlined by Mortlock and Froelich (1989). Briefly, 25 to 100 mg samples were weighed in 50 ml centrifuge tubes and reacted sequentially with 30% H_2O_2 and 1N HCL to remove organic matter and carbonates. Silica was then extracted from the sediment by reacting with 40 ml of 2M Na_2CO_3 in an 85 ºC water bath for 5 hours. After 5 hours, the samples were centrifuged and an aliquot was poured into 30 ml plastic containers. Silica concentrations were determined by a UV-Visible Spectrophotometer (Aquamate) at a wavelength of 812 nm. The calibration standards were prepared by dissolving variable amounts Na_2SiF_6 in deionised water. Calibration standards used for determining the concentration of silica ranged from 0.24 mM to 7.2 mM and had a correlation coefficient of 0.9998. Duplicate of select samples were measured and the average and standard deviation determined. The formula weight is determined by multiplying the weight percent silicon by 2.4 assuming a 10% water content which is typical of air-dried sediment (Mortlock and Froelich, 1989).

3.3.4 Stable carbon isotopes and carbon:nitrogen ratios

The stable carbon isotope ratios ($\delta^{13}C$) of the total organic carbon and the carbon to nitrogen ratios (C:N) were measured from decarbonated sediments. Decarbonation consisted of fumigating approximately 2 g of sediments in plastic Petri dishes with 50 ml of 12 N HCl placed in a closed large plastic container for 24 hours. The samples were dried at 50 ºC for another 24 hours and were then transferred to glass vial for storage. The samples were analyzed using a NC 2500 Elemental analyzer coupled to a Finnigan Delta Plus mass-spectrometer by Finnigan Conflo III device at the Andrew W. Breidenbach Environmental Research Center Librarary/ U.S. Environmental Protection Agency in Cincinnati, Ohio. The Elemental analyzer was set to 1020^0 C and the reduction furnace to 700^0 C. The stable carbon isotope values are reported in δ units in per mil (‰) relative to Vienna Pee Dee Belemnite (VPDB) standard for carbon. The precision of the analysis is better than 0.1‰.

3.3.5 Phosphorus

Samples were analyzed for phosphorus at Indiana State University using a five-step extraction procedure (SEDEX) outlined by Ruttenberg (1992) and modified by Anderson and Delaney (2000) and Latimer et al. (2006). A Shimadzu scanning UV-Visible Spectrophotmeter was employed to determine oxide-associated P, authigenic P, detrital P, and organic P colorimetrically using molybdate blue. Total P was determined after the samples were ashed at 550°C and extracted with 2 M HCl. The authigenic and detrital P concentrations were summed and are referred to as mineral P ($P_{mineral}$).

3.3.6 Inorganic and organic carbon

Sample analysis for total inorganic (C_{inorg}) and organic carbon (C_{org}) was perfomed on the samples using a UIC CM5014 Coulmeter with a CM5130 Acidification Module and a CM5300 Furnace Module. To determine the C_{inorg} CO_2 was released and electronically titrated from a pre-weighed sample by reacting with 2N H_2SO_4. The total carbon was measured by combusting a pre-weighed sample at 950°C in the furnace module. The C_{org} was determined from the difference between the total carbon and C_{inorg}.

3.3.7 Optically stimulated luminescence dating

Optically stimulated luminescence (OSL) dates were obtained at the Oklahoma State University Radiation Dosimetry Laboratory. Samples were prepared under controlled red light conditions. The samples were sieved and then treated with HCL and H_2O_2 to isolate the quartz fraction. The outer surface of the quartz grain was cleaned and etched with 40% HF for 50 min and then re-treated with HCl to remove the fluoride precipitates. Density separation using sodium polytungstate separated out the quartz from heavier minerals and the feldspars. Measurements were obtained from a Risø TL/OSL-DA-15 reader (Risø National Laboratory) with a bialkali PM tube (Thorn EMI 9635QB) and Hoya U-340 filters (290-370 nm). The built-in $^{90}Sr/^{90}Y$ beta source gives a dose rate of 105.7 mGy/s (error 4.1 %). Blue LEDs (470 nm), were used for optical stimulation, delivering 45 mW/cm^2 to the sample; IR stimulation was from an IR LED array at 875 ± 80 nm with 36 mW/cm^2 power at the sample. The heating rate used was 5 ℃/s.

The single aliquot regenerative-dose (SAR) measurement procedures are outlined by Murray and Wintle (2000) and Wintle and Murray (2006). A 5% error was assumed for the cosmic dose rate and an average water content of 10% was assumed. An error of 6% was used for the dose rate calculation. The sample ages in calendar years (referring to 2008) were calculated by dividing the dose by the dose-rate.

CHAPTER 4

RESULTS

4.1. Lithology

The lithologic section from the MABX trench is divided into 5 Units based on lithologic changes (Fig. 3). The Munsell color descriptions of the sediments composing the lithologic units are presented in Appendix A1. The Units are defined as packages of clay- and silt-dominated sediments overlain by intervals with high concentrations of diatomaceous sediment. Unit 1 extends from the base of the lithologic section at 560 cm to 520 cm depth. This unit is capped by a diatom-rich layer of 10 cm thickness. The lower 50 cm of Unit 1 is identified as a light brownish gray sandy clay silt (560 to 530 cm). The overlying diatomite consists of two 5 cm layers of light brownish gray silty diatomite and gray clayey diatomite.

In Unit 2 (520-375 cm) the sandy -clay -silt sediments at the base of the unit account for only 35 cm of the total thickness and consist of light brownish gray clayey silt (520-505 cm) and a light brownish gray sandy -clay -silt (505-485 cm) (Fig. 3). Unit 2 has 145 cm thick accumulation of diatomite (485-375 cm). The diatomite is separated into five intervals. The lower most diatomite interval is light brownish gray diatomite between 485 and 480 cm, the next is a light gray diatomite between 480 and 470 cm. This is overlain by a 50 cm of a white diatomite (470-420 cm) and then another light gray diatomite (420-395 cm). The final interval is 20 cm of white diatomite (395-375 cm). Two OSL dates obtained in Unit 2 give ages of 64.8 ± 4.7 ka at the base of the Unit (500 cm depth) and of 41.31 ± 2.7 ka for the top of the Unit (380 cm depth).

Unit 3 extends between 375 cm to 195 cm depth (Fig. 3). Light brownish gray clayey silt (375 and 350 cm) is overlain by a sandy layer. Unit 3 has 145 cm of accumulation of diatomaceous sediments the thickest in the lithologic section. Light gray clayey- silty- diatomite is at 335 to 310 cm and is overlain by 10 cm of light brownish gray diatomite (310-300 cm). Above the diatomaceous clayey-silt is another light gray diatomite (300-280 cm) and a white diatomite (280-240 cm) interbedded with is a thin clayey-silt interval at 255-250 cm and then another white diatomite. A light gray clayey silty diatomite between 240-195 cm is interrupted by an interval of light brownish gray clayey silty diatomite (230-215 cm).

Unit 4 is 85 cm thick (195-110 cm) and has an OSL age of 26.9 ± 2.0 ka at 135 cm depth in a diatomite layer (Fig. 3). Between 195 and 150 cm is a light gray to gray silty interval with clay clasts. Above this interval is dark gray clay (150-140 cm). The 30 cm-thick diatomaceous interval in Unit 4 is thinner than that of Unit 2 and Unit 3. The diatom rich sediments in Unit 4 includes light gray diatomite (140-120 cm), and light gray diatomaceous clayey-silt (120-110 cm).

Unit 5 (110-5 cm) is the only unit that does not have significant accumulation of diatomaceous sediments (Fig. 3). Unit 5 consists of 35 cm of gray clayey-silt (110-75 cm) that is overlain by a 75 cm-thick layer of dark gray organic-rich sediments that extends from 75 cm to the top of the sedimentary column. The organic-rich sediments have an OSL age date of 11.70 ± 0.9 ka at 45 cm depth (Fig. 3).

4.1.1 Dry bulk density

The dry bulk density values are presented in Appendix A2 and shown in Fig. 3. The values range from 0.36 to1.20 g/cm^3. Dry bulk density values that correspond to layers with higher diatomite content in Unit 2 and Unit 3 have values in the range of 0.36 - 0 .40 g/cm^3. Intervals without a significant occurrence of diatomite have dry bulk density values above 0.90 g/cm^3.

Unit 1 has high dry bulk density values that range from 1.05 to 0.92 g/cm^3 between 560 and 530 cm depth. Between 525 cm and 520 cm depth, the values slightly decrease to 0.83 g/cm^3 in the diatom-rich interval.

In Unit 2, the dry bulk values generally increase between 515 and 480 cm (0.96 to 1.02 g/cm^3). The values then decrease between 480 and 465 cm (0.78 and .037 g/cm^3) concomitant to the presence of diatomaceous sediments. The values from 465 through 420 cm remain about the same, averaging 0.38 ± 0.02 g/cm^3. From 420 to 390 cm, the dry bulk density values increase from 0.41 to 0.714 g/cm^3 and are then followed by a decrease in the values between 385 and 370 cm to 0.34 g/cm^3.

In Unit 3 the dry bulk values are increased from 370 cm to 340 cm and the values range from 0.69 to 1.10 g/cm^3. The values decrease between 340 and 325 cm from 0.90 to 0.54 g/cm^3. Between 325 and 195 cm the dry bulk density can be divided into three distinct intervals (325 to 285 cm, 285 to 240, and 240 to 195 cm). Between 325 to 285 values average 0.64 ± 0.13 g/cm^3, values decrease between 280 and 240 cm averaging 0.38 ± 0.15 g/cm^3, and finally values increase between 240 and 195 cm averaging 0.75 ± 0.08 g/cm^3.

In Unit 4 the dry bulk density values are increasing from 190 cm to 145 cm (from 0.72 to 1.13 g/cm^3). The values then decrease from 1.13 g/cm^3 at 145 cm to 0.511 g/cm^3 at 130 cm. There is then a general increase to the top of the unit

(130 to 110 cm) from 0.511 to 0.90 g/cm^3. The dry bulk density values generally increase throughout Unit 5 from 0.90 g/cm^{3}at 110 cm to 1.17 g/cm^3 at 5 cm.

4.1.2 Inorganic Carbon

The inorganic carbon (C_{inorg}) results are presented in Appendix A2 and shown in Fig. 3. Overall the C_{inorg} varies little (0-0.12 wt. %). The C_{inorg} record is dominated by three increases in C_{inorg}. The first of the increases is at 390 cm depth where C_{inorg} increases from 0.02 wt. % at a depth of 395 cm to 3.24 wt. % at 390 cm followed by a decrease to 0.00 wt. % at 385 cm depth. The next increase in C_{inorg} is between 270 cm and 230 cm depth from 0.24 to 3.49 wt. %. The C_{inorg} values decrease to a low for 10 cm (230-220 cm; ranging between 0.01 and 0.06 wt. %) before increasing between 220 cm and 200 cm depths. This spike in the inorganic carbon (0.91 wt. %) is smaller in magnitude than the first two.

4.2 Chemistry of the sediment leachate

4.2.1 Electrical conductivity and pH of sediment leachate

The results of electrical conductivity and pH of the sediment leachates are presented in Appendix A2 and shown in Figure 4. The electrical conductivity values change little in Unit 1. The values range between 2.2 and 3.2 (mS/cm)/kg except for an increase at 520 cm to 7.6 (mS/cm)/kg. In Unit 2 the electrical conductivity values are high between 520 and 505 cm with values between 5.3 and 10.1 (mS/cm)/kg; with the exception being 510 cm where values decrease to 2.9 (mS/cm)/kg. Above this interval of relatively high values is a decrease that remains generally unchanged between 500 and 410 cm averaging 2.2 ± 2.9 (mS/cm)/kg. The electrical conductivity values fluctuate between 405 and 375 cm ranging from 1.8 (mS/cm)/kg at 390 cm to 18.3 at 3800 cm. The interval at the beginning (370 to 325 cm) of Unit 3 has relatively low and unchanging electrical conductivity values (average; 2.1 ± 1.6 (mS/cm)/kg). Following this depth interval of 370 to 325 cm, the electrical conductivity values begin to increase up to 205 cm depth (23.7 (mS/cm)/kg). The increasing values (320-205 cm) fluctuate frequently and the values range from 3.6 (mS/cm)/kg at 220 cm depth to 23.7 (mS/cm)/kg at 205 cm depth. At the top of Unit 3 and into Unit 4 the electrical conductivity values overall decrease (200 to 145 cm depth; 15.5 to 2.2 (mS/cm)/kg)). At top of Unit 4 (140 to 130 cm depth) the electrical conductivity values fluctuate between high and low, with the maximum at 130 cm depth (16.9 (mS/cm)/kg) and the minimum at 135 cm depth (2.9 (mS/cm)/kg).

Unit 5 has generally low electrical conductivity values (2.3 ± 2.3 (mS/cm)/kg) except at 105 cm depth (8.4 (mS/cm)/kg), 85 cm depth (7.6 (mS/cm)/kg) and 10 cm depth (5.7 (mS/cm)/kg).

The pH in Unit 1 is relatively low and unchanging between 560 and 530 cm depth (7.7 ± 0.1). The pH values then increase slightly through the rest of Unit 1 (525-520 cm-depth) and range from 8.16 at 525 cm to 8.77 at 520 cm depths. In Unit 2 the values are in generally relatively high for this unit between 515 and 480 cm depth (average; 8.07 ± 0.8). The pH values then decrease from 8.39 at 480 cm depths to 7.18 at 470 cm depth. The pH values generally increase in Unit 2 from 470 to 390 cm depths (7.18 to 9.44, respectively). Between 385 and 375 cm depths, the pH values decrease to 8.18 and then increase to 8.84. In Unit 3 the pH values are relatively low for the unit between 370 and 345 cm depth where the values average 8.0 ± 0.4. The pH values then begin to increase between 340 and 205 cm depth from 7.98 to 9.47. In Unit 3 the pH values fluctuate with a range of 7.75 at 110 cm depth to 9.45 at 130 cm depth. The pH values overall are decrease slightly in Unit 1 (averaging 7.69 ± 0.9) except the pH values increase at 85 and 80 cm depths (8.67 and 8.57, respectively).

4.2.2 Cation concentrations

The major cations Ca, Mg, Na, and K are presented in Appendix A2 and are shown and shown in Figure 4. The Ca and Mg concentrations show synchronous variations with depth, and also shift in-phase with the electrical conductity and pH values. Ca and Mg concentrations vary little throughout Unit 1 and Unit 2. However, two intervals (520 to 510 cm depth and 400-385 cm depth) show marked increases in Ca and Mg concentrations. The increase between 525 and 520 is at the top of Unit 1 (0.21 to 0.98 mg/kg and 0.05 to 0.19 mg/kg, respectively). The increase in Ca and Mg concentrations from 400-385 cm depth (0.17 to 2.80 and 0.4 to .27 mg/kg, respectively) is paralleled by increases in the electrical conductivity and pH values. At the base of Unit 3 (375-325 cm) Ca and Mg concentrations are low averaging 0.20 ± 0.1 and 0.05 ± 0.03 mg/kg, respectively. Values increase generally for most of the remainder of Unit 3 (325-210 cm depth) with the minimum for Ca concentrations 0.19 mg/kg and 0.04 for Mg concentrations at 325 cm depth and the maximum for Ca concentrations 3.04 at 220 cm depth and 0.30 Mg concentrations at 215 cm depth. In Unit 4, the Ca and Mg concentrations decrease from 2.48 to 0.21 mg/kg and 0.21 to 0.05 mg/kg, respectively upsection to 150 cm depth, where the clay interval ends. The concentrations of Ca and Mg then increase slightly to 2.47 and 1.18 mg/kg, respectively to the top of the Unit. In Unit 5 there is little variation in the Ca and

Mg values (averaging; 0.17 ± 0.19 mg/kg for Ca and 0.05 ± 0.05 mg/kg for Mg) except for an increase at 85 cm depth (0.98 and 0.14 mg/kg, respectively).

Na and K concentrations vary upsection. Unlike the Ca and Mg concentrations, variations in Na and K concentrations do not closely mirror the variations in the electrical conductivity and pH values. In Unit 1 Na concentrations remain relatively unchanged, from 0.05 to 0.07 mg/kg. In Unit 2 (520 to 375 cm depth) Na varies minimally averaging 0.04 ± 0.03. In Unit 3 the Na concentrations fluctuate but are increasing overall from 0.03 to 0.13 mg/kg (375-210 cm depth). The Na concentrations decrease in Unit 4 from 295 to 415 cm depth (0.05 to 0.01 mg/kg, respectively). The concentrations then increase from 0.01 to 0.13 mg/kg throughout the rest of the Unit into Unit 1 at 85 cm depth. The Na concentrations then systematically decrease to 0.00 mg/kg at 10 cm depth before an increase to 0.07 at 5 cm depth.

The K concentrations vary little ranging from 0.18 to 0.23 mg/kg except for an increase to 0.29 mg/kg at 520 cm depth in Unit 1. In Unit 2 the K concentrations fluctuate between 520 and 460 cm depth but overall the concentrations are decreasing from 0.29 to 0.13 mg/kg. The K concentrations increase through the rest of the unit with the maximum value (0.24 mg/kg) at 395 cm depth. The K concentrations in Unit 3 are increasing in general, but fluctuate frequently. The minimum K concentration occurs at 345 cm depth (0.09 mg/kg) and above this depth, the concentrations increase to 0.38 mg/kg at 200 cm depth. In Unit 4 the K concentrations continue to fluctuate but overall decrease from 0.36 mg/kg at 190 cm depth to 0.23 mg/kg at 110 cm depth. In Unit 5 K concentrations increase from 0.19 mg/kg at 95 cm depth to 0.39 mg/kg at 80 cm and then decrease to 0.19 mg/kg at 70 cm depth. K concentrations again increase depth from 50 cm depth (0.20 mg/kg) to 10 cm depth (0.57 mg/kg) and decreases sharply at 5 cm depth.

4.2.3 Anion concentrations

The results of the major anions HCO_3, SO_4, and Cl are presented in Appendix A2 and shown in Figure 5. In Unit 1 the HCO_3 concentrations very little and range between 1.60 and 4.22 mg/kg. In Unit 2 HCO_3 is elevated between 520 cm depth and 475 cm depth (values range from 2.14 to 4.22 mg/kg), and then decrease between 470 and 400 cm depth to relatively lower HCO_3 values ranging from 0.99 to 2.27 mg/kg. There is a marked increase in HCO_3 values between 400 and 380 cm that peaks at 8.06 mg/kg at 390 cm depth. This spike at 390 cm depth is at the same depth as the spike in the the C_{inorg} and Ca and Mg concentrations (Fig. 3, and Fig. 4). In Unit 3 there is a large increase in HCO_3 values between 325 cm and 250 cm depth that ranges from 1.88 to 12.06

mg/ kg. Below 325 cm depth, the HCO_3 concentrations vary little and have small range (1.88 to 2.27 mg/kg). After the dramatic increase in the HCO_3 concentrations, there is an overall decrease that continues to 145 cm depth (1.64 mg/kg) in Unit 4. In Unit 4 the HCO_3 values decrease from 195 to 145 cm depth and then are higher between 145 and 110 cm depths. The increased concentrations of HCO_3 fluctuate from high to low between 145 and 110 cm depths and range from 1.57 to 8.17 mg/ kg. In Unit 5 the HCO_3 varies little. There is a small spike in the HCO_3 concentrations from 2.02 to 4.71 mg/kg at 85 cm depth. The range in concentrations of HCO_3 in Unit 5 is 1.34 to 4.71 mg/kg.

The SO_4 concentrations also exhibit little change in Unit 1 (4 to 5 mg/kg x 10^{-3}). The SO_4 concentrations in Unit 2 remain low at values from 2 to 7 mg/kg x 10^{-3} except for two spikes at 465 cm and 405 cm depths (26 and 22 mg/kg x 10^{-3} respectively). The SO_4 concentrations increase up in Unit 3 to 285 cm (4 mg/ g x 10^{-3} at 375 cm to 20 mg/kg x 10^{-3} at 285 cm), and then decreases to 225 cm depth (4 mg/kg x 10^{-3}). At the top of Unit 3, SO_4 concentrations again increase between 225 to 215 cm depth (4 to 20 mg/kg x 10^{-3}) and decreases to 7 mg/kg x 10^{-3} at 185 cm depth in Unit 4. The SO_4 concentrations in Unit 4 increases from 185 to 125 cm depths but fluctuate between higher and lower values (5 to 25 mg/kg x 10^{-3}). Unit 5 shows an increase in SO_4 between 95 and 60 cm depths that varies from 5 to 18 mg/ kg x 10^{-3} and another increase at the top of the Unit 1 between 20 cm depth (4 mg/ kg x 10^{-3}) and 15 cm depth (11 mg/kg x 10^{-3}).

Cl concentrations increase in Unit 1 and unit 1 fluctuate from 1 to 4 mg/kg x 10^{-3}, and show no consistent variations. In Unit 3 Cl in general remains unchanged, ranging from 1 to 4 mg/kg x 10^{-3} with the exception of an increased spike at 315 cm depth (8 mg/kg x 10^{-3}). The noticeable variation in the Cl data is a spike at 155 cm depth (7 mg/kg x 10^{-3}). Although the Cl concentrations fluctuate frequently, there is a general increase upward in Unit 5 and values range from 4 mg/kg x 10^{-3} to 9 mg/kg x 10^{-3}.

4.3. Phosphorus

The results of the P measurements are presented in Appendix A2 and shown in Figure 6. The phosphorus record is dominated by elevated values between 290 and 190 cm depths in Unit 3. The P concentrations increase from 1.00 μmol/kg*10^3 to 37.29 μmol/kg*10^3 at 210 cm depth. This increase in P_{total} concentration is a result of a large increase in the $P_{mineral}$ component from 0.99 to 37.29 μmol/kg*10^3 between 210 and 190 cm depth. The magnitude of the values in Unit 3 suppresses smaller scale changes in the rest of the P record. Graphs of P_{total} and $P_{mineral}$ in Figure 6 have been expanded to exclude the section between 290 and 190 cm depths in order to emphasize these changes. The expanded

graph sections show that there is no change in the phosphorus values in Unit 1 (~1.00 μmol/kg*10^3). The P_{total} values increase in Unit 2 between 520 and 460 cm depths to 5.48 μmol/kg*10^3. The values decrease to a range of ~2.5-3.0 μmol/kg*10^3 between 460 and 380 cm depths. There are two spikes in the P_{total} concentrations in this Unit at 420 and 390 cm depths (4.12 and 7.98 μmol/k*10^3, respectively). The increases in P_{total} in Unit 2 are associated with increases in the $P_{mineral}$ component (470 cm: 2.87 μmol/kg*10^3, 420 cmdept; 3.22 μmol/kg*10^3, and 390 cm depth; 5.91 μmol/kg*10^3). The spike at 390 cm depth occurs at the same depth as observed increases in the electrical conductivity and pH values, and Ca, and Mg concentrations (Fig. 4). P_{total} concentrations in Unit 4 are decreasing overall from 5.75 μmol/kg*10^3 at 190 cm depth to 2.19 μmol/kg*10^3 at 125 cm depth. The P_{total} concentrations then increase into Unit 1 at 80 cm depth (6.06 μmol/kg*10^3). The values for P_{total} above 80 cm depth decrease to 20 cm depth (0.87 μmol/kg*10^3) and then increase in the last 15 cm to a maximum of 5.40 (3.79 μmol/kg*10^3 at 15 cm depth. The $P_{mineral}$ concentrations decline from 80 cm depth (2.43 μmol/kg*10^3) to the top of the core at 5 cm depth (3.43 μmol/kg*10^3)

Normalized abundances of the three P phase components mineral-, organic-, and oxidized-P) are also shown in appendix A2. Mineral- and organic-P are inversely related. Generally, oxide-bound P is not a significant component of the total P.

4.4 Opal

The opal results are presented in Appendix A2 and shown in Figure 7. Opal concentrations closely correspond to the sediment lithologies. Opal concentrations are highest in the diatom-dominated intervals (Fig. 3 and Fig. 7), with values ranging between 26 and 58 wt. % in these intervals. Lithologic layers that are dominated by silt or clay tend to have opal concentrations that range between 8 and 10 wt. %. The organic-rich sediments have opal values ranging from 9 to 17 wt. %.

In Unit 1 opal concentrations do not vary and are from about 14 to 17 wt. %. Unit 2 the opal concentrations remain relatively low, concomitant with the clayey-silt and sandy clay silt interval. Concentrations increase above 485 cm depth in Unit 2 from 14 to 53 wt. % at 450 cm depth and are relatively high until 360 cm depth at the top of Unit 2. The opal concentrations decrease from 360 to 345 cm depth (47 to 10 wt. %) in Unit 3. The opal concentrations again increase above 345 cm depth and are relatively high throughout the rest of the Unit (195 cm depth). The opal concentrations decrease in Unit 4 to 9 wt. % at 145 cm depth from 40 wt. % at 190 cm depth. Opal concentrations increase to 38 wt. %

from 145 to 125 cm depths. The opal concentrations then decrease to 22 wt. % at 110 cm depth. In Unit 5 opal concentrations continue to decrease to the top of the unit and range from 27 to 10 wt. %.

4.5 Organic matter, carbon to nitrogen ratios, and the stable isotope composition of organic matter

The organic matter (C_{org}), C:N ratios, and $\delta^{13}C_{org}$ results are presented in Appendix A2 and shown in Figure 7. Unlike opal concentrations, C_{org} concentrations do not systematically vary with lithology. Organic carbon concentrations are generally low throughout most of the lithologic section, ranging between 0.08 and 0.42 wt. % from 560 to 240 cm depth. There is a spike in Unit 3 at 265 cm depth where the C_{org} values increases to 1.47 wt. %. Within Unit 4 and Unit 5, C_{org} generally increases upsection. There are three distinct increases upsection separated by slight decreases in the $C_{org.}$ The first of these three sections is from 195 to 145 cm depth where C_{org} increases from 0.16 to 0.93 wt. %, the second section is between 140 and 105 cm depth where C_{org} increases from 0.43 to 1.26 wt. %, and the third increase in the C_{org} occurs from 100 to 10 cm depth where C_{org} increases from 0.61 to 2.58 wt. %.

The C:N ratios exhibit little variation at depths below 250 cm (Unit 1, Unit 2, and Unit 3), ranging between 0 and 5 (Fig. 7). The only exception is a spike in the values is 22 which occur between 435-420 cm depths. From 240 to 210 cm depth, C:N ratios increase from 3 to 9, coincident with observed high values in the electrical conductivity, pH, Mg, and Ca in the sediment leachate(Fig. 4) and $P_{mineral}$ (Fig.6). In Unit 4 and Unit 5, C:N ratios increase from 200-145 cm, 140-105 cm, and 100-10 cm depths. From 200-145 cm depths the values increase from 2 to 12. This interval is concurrent with the silty and clayey layers in the lithologic record (Fig. 3). The values between 140-105 cm depths increase from 3 to 15. The lower values in this interval correspond to an increase in the diatom rich sediments. The 100-10 cm depth interval begins with low C:N ratios (100-55 cm depth at ~8) which then increase to 25 in the top 10 cm. The lower C:N values correspond to the clayey-silt rich sediments and the higher values at the top of the unit are rich in organics.

The isotopic composition of the organic carbon ($\delta^{13}C_{org}$) does not vary with lithology. $\delta^{13}C_{org}$ values in Units 1 and Unit 2 vary between -21.6 and -17.7 ‰, but no discernable trend with depth is evident in Unit 1; however, values overall decrease in Unit 2. $\delta^{13}C_{org}$ values generally decrease in Unit 3, but become more negative from -18.9 to -23.6 ‰ to -18.9 ‰ from 265 to 210 cm depth within Unit 3. This shift occurs concomitant to the thin clayey silt interval and the thick clayey silty diatomite of Unit 3 (Fig. 3). At the depth of 265-210 cm, the electrical

conductivity, pH, Mg, Ca, HCO_3, inorganic carbon, and $P_{mineral}$ values are relatively high (Fig. 3, Fig. 4, Fig. 5, and Fig. 6). The $\delta^{13}C_{org}$ values shift to less negative values (−23.5 to –17.0 ‰) at the top of Unit 3, and remain high (–18 to −17‰) throughout the silt- and clay-dominated layers in Unit 4. The $\delta^{13}C_{org}$ values then decrease from –17.09 ‰ to –22.0 ‰ from 145 to 90 cm depth in Unit 5. From 90 cm depth to the surface, $\delta^{13}C_{org}$ values shift to less negative values (−22.0 ‰ to –16.1 ‰), which also corresponds to the slight increase in C_{org} concentrations.

CHAPTER 5

DISCUSSION

5.1. Sedimentation and relative lake levels in Paleolake Mababe

The sedimentation record indicates that lacustrine conditions have persisted in the Mababe Depression for the past ~65 ka. Lake sedimentation was cyclic for the majority of the record, with accumulations of diatomaceous sediments nested within intervals dominated by sands, silts, or clays (Fig. 3). The sands, silts, and clays were delivered into Paleolake Mababe by four main rivers (Fig. 2). The Mababe River linked to the Okavango and the Savuti River linked to the Kwando, both of which drain distal watersheds in the Angolan highlands in the tropics. The Ngwezumba and Guatumbi Rivers drain local watersheds in the Kalahari Basin to the northeast of the Mababe Depression. Variations in the mineralogical composition of the detrital sediments are attributed to a change in the relative contribution from the different watersheds. The sands derived from local watersheds are eolian and belong to the Kalahari Group (McCarthy et al., 2002; Gamrod, 2009). The silt and clay are thought to be dominated by sediments eroded from watersheds in the Angolan highlands (Gamrod, 2009). In contrast, diatomaceous sediments accumulated from the remains of diatom blooms in the paleolake, so the preservation of thick accumulations indicates that the lake remained relatively stable for extended periods of time. Unit 2 and Unit 3 represent the longest time intervals of stable lacustrine conditions, because of the thick diatom deposits (Fig. 3 and Fig. 7). The diatomaceous intervals have low amounts of mineral sediments, especially sand. The absence of sand is telling, as this suggest that the river discharge sustaining lake levels during the accumulation of diatoms was likely sourced from the Angolan highlands (Gamrod, 2009). The composition of the sediments and diatom abundance indicate that relatively stable lake conditions occurred from 65 ka to about to slightly younger than 27 ka, when the last accumulation of diatoms in the sedimentary record is observed in Unit 4. The lack of diatom

accumulation in Unit 5 suggests generally shallow lake levels or low nutrient conditions that limited diatom growth.

5.2. Chemistry of Paleolake Mababe waters

Sequential leaching of sediments is often used to constrain the sources of different elements preserved in the sedimentary record (Eugster and Jones, 1979; Lent et al., 1995). Water soluble solute composition of the leachate can be used to infer the composition of the mineral salts from theoretical reactions induced by evaporative concentration of lake waters (Sonnefeld, 1984). Changes in the concentration of the different solutes indicate variations in the chemistry of lake water from such processes as rainfall, river discharge, and weathering in the drainage catchment (Eugster and Jones 1979). The salinity of lake water increases and mineral precipitation occurs when evaporation exceeds recharge and the concentration of dissolved ions increases beyond the solubility threshold for different evaporite minerals (Sonnenfeld, 1984).

The electrical conductivity of the leachate can be used to infer salinity variations in Paleolake Mababe, because the electrical conductivity is controlled by the concentrations of solute ions derived from evaporite minerals in the sediment. Increasing salinity in Paloelake Mababe water is recorded as increases in the electrical conductivity values. The first increase in salinity occurred 41 ka ago at the top of Unit 2 between 405 cm to 390 cm depth (Fig. 4). This increase in salinity is concomitant with marked increases in pH and in the Ca and Mg concentrations. In Unit 3 another period of increased salinity is observed over a much longer duration between 41 ka and 26 ka. The electrical conductivity, pH, and Ca and Mg concentrations of the sediment leachate begin to increase steadily from 340 cm until 245 cm depth (Fig. 4). A relatively short (245-230 cm depth) increase in Na lags the increase in Ca and Mg concentrations. There is an appreciable increase in the electrical conductivity at 100 cm to 85 cm depth in Unit 5 between 27 and 12 ka which is accompanied by modest increases in pH, and the Ca and Mg concentrations (Fig. 4). Fluctuations from high to low electrical conductivity in Unit 4 occur between 140 cm and 120 cm depth around 27 ka. The increases in the salinity occur during periods when diatoms are accumulating within the sediments. These results suggest that during the time periods with significant diatom accumulation within the sediment record, lake levels had to be stable to supported extensive diatom growth.

Although the solute concentrations of lakes in the middle Kalahari can increase from groundwater recharge as described by Nash (1997), previous studies suggest that paloelakes in the middle Kalahari were sustained by river discharge (Shaw, 1988; McCarthy and Ellery, 1986; Huntsman-Mapila et al.,

2006; Burrough and Thomas, 2008). Thus, the increase salinity of Paleolake Mababe was the result of evaporative concentration of solutes leading to evaporite formation similar to the evaporite formation during modern climate conditions.

The chemical composition and the relative concentration of solutes in the water recharging the lake ultimately determines the types of minerals precipitated and order of mineral precipitation from evaporative concentration (Sonnefeld, 1984; Eugster and Jones 1979). Also, if the recharge water is depleted with respect to a particular element, then the residence time required for the concentration of the element to the point of saturation to induce precipitation will be longer. Although it is not possible to determine the concentration of water that recharged the lake in the past, it must have varied between that of water from the distal Angolan and from local Kalahari watersheds. River discharge from watersheds in the Angolan highlands is probably similar to that of the modern day Okavango and Kwando Rivers. In the upper panhandle of the Okavango Delta, river water at Mohembo contains 2.5 mg/l of Ca, 2.3 mg/l of Mg, 1.8 mg/l of Na, 1.3 mg/l of K, 0.61 mg/l of Cl, and 0.51 mg/l of SO_4 (E. Atekwana, unpublished). Once in the Okavango Delta, the water becomes preferentially concentrated as a result of evaporative concentration. After the water is evaporated as it passes through the delta, it then contains a solute load represented by the concentrations 10.5 mg/l of Ca, 3.7 mg/l of Mg, 11.6 mg/l of Na, 3.6 mg/l of K, 0.57 mg/l of Cl, and 0.1 mg/l of SO_4 from the Thamalakane River near Maun (E. Atekwana, unpublished). McCarthy and Metcalfe (1990) found that in the Okavango Delta chemical precipitation is limited to bicarbonate minerals with the initial precipitation of Ca bicarbonate and the co-precipitation of Mg and then later in the cycle of brine formation the Na and K bicarbonates precipitate out of the solution. The same study by McCarthy and Metcalfe (1990) indicates that chlorides and sulfate precipitation is absent in the Okavango Delta because of low concentrations in the source waters. Therefore, if the Mababe Depression evaporites are consistent with those observed in the Okavango Delta, the Mababe Depression evaporites should be dominated by bicarbonate minerals and contain minimal Cl and SO_4.

A modern analogue to the brine development of the Mababe Depression is found in the Makgadikgadi Pans to the south. The brine of the Makgadikgadi Pans is predominantly bicarbonate, but is evolving toward a more sulfate rich brine consistent with low initial sulfate concentration in the Okavango River source water (Eckardt et al., 2008). In the Makgadikgadi Pans $CaCO_3$ (calcite; solubility: 0.00014 m/L), $MgCO_3$ (magnesite; solubility: 0.001 m/L) are precipitating out of lake water (Warren, 2006; Eckardt et al., 2008). Na is conserved longer than the Ca and Mg and in the Makgadikgadi Pans; the Na is

precipitated in the shallow littoral zone because the water has become more depleted in Ca and Mg in this zone. The Na is precipitates as NaCl (halite; solubility: 6.15 m/L), $Na_2SO_410H_2O$ (mirabilite; solubility: 1.96 m/L), and $NaHCO_3$ (nahcolite; solubility: 1.22 m/L) (Warren, 2006; Eckardt et al., 2008).

The Ca proportion in the cations leachate from the sediment from the Mababe Depression increase up section while the K proportion decrease concomitantly with increase in Ca (Fig. 8). The proportion of Mg is nearly constant at 20% throughout the section and the Na remains nearly steady at ~10% from the bottom to 80 cm depth, where a slight decrease in the concentration occurs to the top of the section (Fig. 8). The relative proportions of the cations suggest that the bulk of the highly soluble evaporite minerals in the sediment are composed of Ca salts. The anion proportions in the dissolved evaporite minerals show little depth variations in Cl and SO_4, suggesting that HCO_3, which also varies little throughout, is the dominant anion (Fig. 9). There is a positively correlation between Ca and HCO_3 given by the least squares regression equation: $Ca^{2+} = 0.9xHCO_3^- - 0.02$ ($R^2 = 0.97$) indicating that about 90% of the HCO_3 in the solution forms minerals with Ca (Fig. 10). The chemical composition of the evaporite is $Ca(HCO_3)_2$. Also, the formation of $Ca(HCO_3)_2$ is an indication that evaporative concentration in Paleolake Mababe stayed mostly within the saturation point of carbonates. In the upper 80 cm of Unit 1, there is an appreciable decrease in Ca and Na, while K increases in the sediment leachate from below 40% to about 60%. The relative increase in K is likely due to precipitation of K-evaporites such as sylvite (KCl). Although the main evaporites in the sediment leachate are Ca salts, evaporites with composition of Ca-Mg-$(HCO_3)_2$ and Ca-Na-HCO_3 types could be precipitated in the shallow littoral margins of the lake (e.g., Eckardt et al., 2008).

There are three anomalous increases in inorganic carbon and P_{total} values; at 390 cm depth, from 290 cm to 240 cm depth, and from 220 cm to 120 cm depth (Fig. 3 and Fig. 6). Although the carbonate can be explained by precipitation from lake water saturated with carbonate, the chemical saturation of the lake water does not explain the concomitant increase in P_{total}. The bulk of the P_{total} is $P_{mineral}$ derived from weathering of apatite in drainage catchments (Anderson and Delaney, 2001; Latimer et al., 2006). If the anomalous increases in $P_{mineral}$ concentrations indicate increased weathering in the catchment from wetter climate, then its delivery into the lake would also signify increase river discharge from the local Kalahari watersheds or the distal watersheds in the Angolan highlands. Gamrod (2009) suggests that increased C_{inorg} in the sediment record could have resulted from the erosion of calcretes in middle Kalahari watersheds during locally wet climate. Nash (1997) suggests that dissolved Si, Ca, and Mg form carbonates dissected from pre-existing clacretes

can be transported by fluvial systems in the middle Kalahari as dissolved or suspended loads.

The increased values in $P_{mineral}$ could be the result of calcrete erosion. Eckardt et al. (2008) found that some of the calcretes in the Sua Pan to the south of the Mababe Depression contain low levels of P and Kampunzu et al. (2007) found low levels of P_2O_5 (up to 0.04 %) in calcretes in the region. It is suggested that the sediment intervals with anomalously high carbonates are likely a result of erosion of calcrete layers from increased local precipitation and that the increased $P_{mineral}$ is sourced locally from calcrete. The deposition of the mineral salts from increased inflow into Paloelake Mababe is at odds with other mineral salts being deposited in the lake during a negative hydrologic budget caused by evaporative concentration. It has been suggested that during the deposition of the sediments between 290 and 240 cm depth, there was a dramatic alteration in the regional hydrology that caused high levels of fluvial erosion in the local watersheds. The increased erosion can be attributed to increased local precipitation due to a local wet event. Gamrod (2009) suggests that a local increase in precipitation is concurrent to the onset of tectonic activity, and during sedimentation at this depth interval, there was also altered fluvial input into the middle Kalahari lakes by re-direction of the Kwando River along the Linyanti fault and also the initiation of the formation of the modern-day Okavango Delta. If the tectonic activity resulted in uplift and a change in base level of the rivers, then it could have led to increased fluvial incision and erosion of subsurface layers of calcrete. The sediments at depth intervals with anomalously high carbonates are also associated with an increase in silt and clay, but there is an unexplained lack of sand that should accompany sediment erosion from local watersheds (Gamrod, 2009). Sand may not be observed in the trenched location where samples were collected because it could have been deposited in the deltas of the rivers. At 360 cm depth, the lake is fresh interpreted from the low concentrations of evaporite minerals (Fig. 4 and Fig. 5) indicating that water input and lake levels were most likely high. During sedimentation at 325 cm depth, the concentration of Ca, Mg, and HCO_3 began to increase, suggesting that the inflow into Paleolake Mababe was less than the water being lost to evaporation (Fig. 4 and Fig. 5). For sediment erosion to be occurring locally and for sand to not be associated with the calcrete and P, the lake would need to be full enough during sediment deposition at 290 cm depth. This would allow the heavier sand to be deposited nearshore in the deltas and the disseminated calcretes basinward. The lake would have to be full enough prior to sedimentation at 325 cm depth so that evaporation would not desiccate the lake to a level too low for differential deposition of the sediments.

Overall, the data from the sediment leachate chemistry indicates that the water in Paloelake Mababe was less saline during the time interval of Unit 4 and Unit 5. The sedimentary characteristics of Unit 5 are markedly different from the lower units. Here, the cyclicity between mineral sediments and diatoms is interrupted, and the sediment section is mainly silts and clays rich in organic matter. The leachate chemistry shows a continuous decrease in the proportion of Ca and Na, relatively no change in Mg, and enrichment in K. Although the decreasing Ca and Na concentrations are consistent with freshwater, the increase in K is unexplained. It is probable that the residence time of the water in the paloelake during this time was short and evaporative concentration of lake waters did not occur perhaps because the short residence time. Overall, the lake water during this period shows no evaporative enrichment except in the top 10 cm depth where the proportion of Ca and Na increase consistent with the complete desiccation of the lake to the present modern day conditions.

The electrical conductivity, pH, and the cations and anion proportions in the sediment leachate and $P_{mineral}$ data can be used to develop three distinct models of lake water chemical conditions for Paleolake Mababe. The first model represents a lake with freshwater and low solute concentrations. This freshwater and low solute signature is observed in Paloelake Mababe in Unit I and Unit 2 up to 400 cm depth and Unit 3 between 370 and 325 cm depths (Fig. 4 and Fig. 5). The lake hydrology under model 2 has negative lake water balance. This model requires a relatively wet climate in watersheds in the Angolan highlands to maintain river discharge, while locally dry conditions evaporate lake water concentrating ions in solution. The evaporative concentration causes precipitation of evaporites in the sediments. Conditions under model 2 are observed mainly in Unit 3 between depths of 325 cm to 295 cm and in Unit 4 between depths of 150 cm and 135 cm (Fig. 4 and Fig. 5). In model 3, recharge water has a high solute concentration. The high solute concentration of lake water is due to river recharge high in solutes dissolved from the evaporites in soils in the local watersheds. The high solute concentrations in the recharge water eventually led to precipitation of evaporites minerals from evaporative concentration as observed in sediments depths between 395 cm and 385 (Fig. 4 and Fig. 5). River recharge in evaporites and calcretes also causes disproportionate increases in evaporties and inorganic carbon in sediments between 285 cm to 200 cm depths.

5.3. Lacustrine productivity

5.3.1. Biogenic silica

The opal record of Paleolake Mababe sediment reflects extended periods of diatom accumulation in Unit 2, Unit 3, and Unit 4. Deposition of diatomaceous layers of considerable thickness would require the persistence of a stable lake and bottom-water conditions conducive to opal preservation. This suggests that between 60 ka and shortly after 26 ka, lake water conditions were favorable to promote both the growth and preservation of diatoms. Diatom accumulation in Unit 3 and Unit 4 occurred in a lake with elevated salinity deduced from increasing electrical conductivity, pH, and Ca and Mg concentration in sediments (e.g., Fig. 4). Based on the preservation of diatomaceous sediments during these time periods, diatom communities in Paloelake Mababe appear to thrive when lake salinity was high and P (Fig. 6) was not limiting. In Unit 2, however, high opal concentrations occur in a lake water of low salinity. The diatom accumulation begins at 485 cm depth and remains relatively high until about 380 cm depth (Fig. 7). Whereas an increase in the electrical conductivity, pH, and Ca concentration and Mg concentrations from the sediment leachate (Fig. 4) and the $P_{mineral}$ concentrations (Fig. 6) only occur between 390 and 395 cm depth. There is a slight increase in the $P_{mineral}$ concentrations at 520-465 cm depth which decreases to around 1 μmol/Kg$\cdot 10^3$ when the opal concentrations are the highest (465-430 cm depth). The decrease in P is due to utilization by the diatoms. Phosphorus becomes incorporated in the diatom tests and is only released when the tests are dissolved (Kroger et al., 2002). A study by Latimer et al. (2006) found that in some marine sediment with high concentrations of diatoms, the total P could be increased as much as 767 % when opal associated P was accounted for. The low concentrations of P_{total} between 465-430 cm depths do not necessarily mean that there was not a high influx of phosphorus into the lake during this time interval. Because the decrease in P_{total} corresponds to the highest levels of diatom preservation, it suggests that diatom productivity was high enough during this period to extract and incorporate the P into the silica tests. The P_{total} concentrations peaks after opal concentrations decline slightly at 420 cm and 390 cm depths, and suggest the important role of P in the growth of diatoms in the Paloelake Mababe.

The lithology of Unit 2 records an increase in the contribution of water from the watershed into Paleolake Mababe. This inference is made based on the assumption that P concentrations were elevated in the lake but were low in the sediment record because P was sequestered in the diatom tests. The steady increase in $P_{mineral}$ between the depths of 520 cm to 500 cm subsequently declines during rapid diatom growth. Saline conditions are not observed in

progressively younger sediments in Unit 2 until 390 cm depth, suggesting that the lake recharge exceeded evaporation and the diatoms were not dependent on the saline conditions observed in Unit 3 but instead relied more on the availability of P (Fig. 6).

In general, the record from Paloelake Mababe shows a decrease in the opal concentrations above 110 cm depth. This is possibly the result of lake shallowing and change in nutrient levels, making lacustrine condition inhospitable for diatom growth. The low concentration of soluble evaporite minerals in the sediment leachate data suggested that during sedimentation in this upper 110 cm, the residence time of water in the lake was shortened prohibiting the evaporative concentration of ions. If this shorter residence time also corresponded to shallower lake conditions, then diatom growth may have been inhibited. This would indicate that in Paleolake Mababe, significant diatom accumulation was dependent on the depth of the water and the availability of P.

5.3.2. Organic matter

The C_{org}, $\delta^{13}C_{org}$, and C:N ratios indicates that a major shift in lacustrine organic matter productivity and/or preservation in the sedimentary record occurred around 260 cm depth (Fig. 7). Overall, the accumulation of organic matter in sediments begins to increase steadily at ~260 cm depth all the way to the surface. In lacustrine sediments, most of the organic matter persevered is derived from the particulate detritus of aquatic vegetation from terrestrial vegetation growing in the littoral regions, or from the lake catchment brought to the lake by river discharge (Meyers and Ishiwatari, 1993). Higher organic matter concentrations are usually observed in shallower lakes (Wetzel, 2001). Disproportionately higher organic matter from wetlands and the littoral regions is readily preserved in sediments because the organic matter is relatively resistant to bacterial degradation during burial, and there is less time for oxidation to occur while sinking in a shallower water column (Meyers and Ishiwatari, 1993; Wetzler, 2001). Although there is an overall increase in organic matter concentration up section from 260 cm depth, there are four prominent increases in the record between depths of 260 cm to 210 cm, 200 cm to 145 cm, from 140 cm to 105 cm, and 90 cm to 5 cm (Fig. 7). The decreases in organic matter concentration that interrupt the otherwise continuous increases in organic matter represent periods of significant lake deepening. A brief deepening of the lake will eliminate mash- and littoral-type vegetation and submerged aquatic vegetation. Although the predominant vegetation in the deeper lakes is phytoplankton, the rate of accumulation and preservation is lower in the sediment record.

Variations in the C:N ratios with depth closely follow similar increases and decreases observed for organic carbon concentrations. The C:N ratios are <10 for the sedimentary record below 260 cm depth (Fig. 7). The C:N ratios of aquatic plants are low and range from 4 to 10, while the C:N ratios of terrestrial vegetation is ≥ 20 (Meyers and Ishiwataric, 1993), due to differences in cellulose contents. Land plants contain lignin in their cellulose structure which provides structural support, and can contain up to 0.5 wt. % N (Hunt, 1990). Lakes that receive a large proportion of organic matter from wetland or marsh plants have higher organic matter in the sediments, and the C:N ratios will be high, reflective of shallower lake conditions or lakes with a large carbon contribution from the terrestrial settings. Wang et al. (2007) report C:N ratios of 9.9 ±0.2 for the areas under vegetation canopies and 9.1 ± for inter-canopy areas at the Tshane site with acacia savanna vegetation similar the acacia parkland in the Mababe Depression (Shaw, 1985). Thus, the C:N ratios from Wang et al. (2007) provide terrestrial end-member values for C:N ratio that represent the current environmental conditions of the Mababe Depression.

Variations in $\delta^{13}C_{org}$ values are a result of the preferential incorporation of either ^{12}C or ^{13}C into organic carbon through the C3 Calvin-Benson pathway or the C4 Hatch-Slack pathway, respectively (O'Leary, 1981; Meyers and Ishiwatari, 1993; Krishnamurthy et al., 1998; Beuning et al. 2003; Muzuka et al., 2004). The incorporation of the isotopically heavier ^{13}C shifts the carbon isotopes values more positive relative to the VPDB standard (O'Leary, 1981). The mean $\delta^{13}C_{org}$ values for C3 plants are ca -28‰ and for C4 plants is ca -14‰ (O'Leary, 1981; Meyers and Ishiwatari, 1993). Positive shifts in $\delta^{13}C_{org}$ represent an increase in the amount of organic carbon derived from C4 plants. Since C4 plants dominate in arid environments, this shift is usually interpreted as evidence for a climatic shift toward a more arid climate (Meyers and Ishiwatari, 1993; Muzuka et al., 2004).

The sediment record from the 560-260 cm depth shows that the values for the $\delta^{13}C_{org}$ in the sediments from the lower 260 cm depths ranges from ~ -22 to -18 ‰ and from -23.5 ‰ to -16 ‰ in the sediments of the upper 260 cm depths (Fig. 7). The wider variation in the $\delta^{13}C_{org}$ values in sediments above 260 cm depths indicated a much greater variation in the source of the organic matter compared to deeper depths. Also, the periodic increases in the organic matter described for the upper 260 cm depths do not all correspond to the same shift in the $\delta^{13}C_{org}$ (Fig. 7). The increase in organic matter concentration between depths of 260 cm to 210 cm is accompanied by negative shift in $\delta^{13}C_{org}$, 200 cm to 140 cm depth by a positive shift in $\delta^{13}C_{org}$, 135 cm to 105 cm by a negative shift in $\delta^{13}C_{org}$, and 90 cm to 5 cm by a positive shift in $\delta^{13}C_{org}$. Wang et al. (2007) measured the $\delta^{13}C_{org}$ values of a vegetation community in the middle Kalahari

that is similar to that of the Mababe region and report $\delta^{13}C_{org}$ values that range from -12.8 ±0.6 ‰ to -18.5 ±1.1 ‰. Shifts to more positive values in the organic carbon isotope record are consistent with more arid environmental conditions arid similar to the present. The shifts to higher $\delta^{13}C_{org}$ values may also be the result of a shift to increased C4 plants in the wetlands of the watersheds. Mladenov et al. (2007) reports that in the Okavango Delta, C4 plants like the Cyperus papyrus and Panicum repens are found in the permanent and seasonal swamps.

The variation in organic matter can be interpreted in the sediment record above 260 cm depths. From 260 cm to 210 cm depths, the C_{org} and C:N ratios increase and the $\delta^{13}C_{org}$ values decrease (Fig. 7). The organic matter preserved in Paleolake Mababe during this interval is increasing from vascular plants and the proportion of C3 to C4 plants is increasing. This interval represents the first significant increase in organic material and C:N ratios in the record. At this depth, there is also a significant increase in C_{inorg}, P, and evaporite mineral deposition (Fig. 5, Fig 6, and Fig. 7). The increase in the deposition of the C_{inorg}, P, and evaporite minerals is attributed to increased erosion in the watershed due to tectonic activity and locally increased precipitation. The increase in organic matter and C:N is also a result of the increased transport of organic matter from vascular plants into the lake. Gamrod (2009) suggested that at this depth interval, the Okavango Delta began to form. The formation of the Okavango Delta could provide a source for the vascular plants. The locally wet climate and high lake levels supported an environment dominated by C3 vegetation.

Between 210 and 200 cm depths, the C_{org} and C:N ratio decrease indicating a shift to a more aquatic system, but $\delta^{13}C_{org}$ values sharply begin to increase indicating more C4 vegetation typical of a more arid vegetation shift. During this interval, it is likely that C4 plants are a large component of the wetland vegetation. The values of $\delta^{13}C_{org}$ increase to around -16 ‰ (Fig. 7). The C. papyrus, and P. repens found in the Okavango Delta have $\delta^{13}C$ values of -11.6 ‰ and -12.2 ‰ respectively (Mladenov et al., 2007). Overall the C_{org} and C:N ratios indicate a decrease in the amount of vascular material entering Paleolake Mababe, but C4 plants like C. papyrus, and P. repens are likely to be the vascular plants that are being deposited into the lake. If the interval represents a more arid climate, then the decrease in vascular plants in the sediment record could in part be the result of decreased fluvial transport of vascular plants.

The next time interval in for increased organic matter is from 200 to 145 cm depths. The top of this interval is near 27 ka and is characterized by increasing C_{org} values and C:N ratios, and high, but relatively unchanging $\delta^{13}C_{org}$ values. The interval represents an increase in vascular plants that are

predominantly C4. These variations are consistent with the modern signature of the Mababe Depression and could represent a shallowing of the lake. This increase in the C_{org} and C:N would be the result of increased vascular vegetation from the littoral regions of the lake and the development of marsh/wetland vegetation on the lake margins. The C4 vegetation indicates the climate may have been more arid and this could account for the shallower lake conditions.

At 145 cm depth, the C_{org} values, C:N ratio, and the $\delta^{13}C_{org}$ all begin to decrease. The C_{org} and C:N ratios remain low until 120 cm depth and then begin to increase (Fig. 7). The C_{org} values and C:N ratios increase from 120 cm to 105 cm depth (Fig. 7). The $\delta^{13}C_{org}$ values decrease throughout the interval (145-105 cm depths). The initial decrease and low C_{org} concentrations and C:N ratios reflects a decline in vascular plants and signifies a possible deepening of the lake. The decrease in the $\delta^{13}C_{org}$ indicates that C3 type plants are becoming more abundant then the C4 type plants. This could be the result of increased aquatic productivity and vegetation in the watershed being preferentially C3 type plants. A deepening of the lake is also apparent in the biological productivity data. This decrease in the organic productivity data is concomitant to an increase in the % opal data which is interpreted as result of deeper stable lake conditions (Fig. 7).

The increase in the C_{org} and C:N ratios at 120 cm depth indicates more organic matter from vascular plants are being deposited in the Paleolake Mababe (Fig. 7). This organic matter is dominated by C3 type plants as reflected in the continued decrease in the δ^{13} C_{org} values. Paleolake Mababe deepened between 145 and 120 cm depth according the organic matter proxies, and then began to shallow between 120 and 105 cm depths. The shallower lake probable saw the encroachment of marsh and wetland vegetation into Paleolake Mababe that is dominantly C4 type vegetation.

After this cycle of deepening and shallowing there is again another decrease in the C_{org} and C:N ratios. Between 105 and 90 cm depths, the C_{org} and C:N ratios decrease, and the $\delta^{13}C_{org}$ continues to decrease indicating that less organic matter is being sourced from vascular vegetation to Paleolake Mababe, and that the organic matter deposited is dominated by C3 plants (Fig. 7). This could be an indicator of deeper water conditions and less littoral vegetation or a decrease in the organic matter input from the watershed because of decreased fluvial transportation of vascular detritus. The decrease in the C:N ratio is around 9 which is consistent with values given by Wang et al. (2007) for environments in Botswana similar to those of the present day Mababe Depression. Because the C:N ratios remain relatively high, it is more likely that the decrease is due to less vascular plant material being delivered to Paleolake Mababe instead of a deepening of the lake.

The sediment record between 90 and 5 cm depths indicate that the C_{org}, C:N ratios and $\delta^{13}C_{org}$ values are all increasing overall to the present day values. This reflects an increase in the deposition of vascular organic matter and an increase in the proportion of C4 plants to C3 plants. This is thought to be a steady decline in lake levels of Paleolake Mababe and the final desiccation of the lake. This time interval probably represents a transition from a shallow aquatic setting to a widespread marsh/wetland, and finally to an acacia parkland environment. There are possible shifts toward wetter climate and/or deeper lake conditions in the intervals from 70-60 cm, 50-40 cm, and 30-20 cm depths. However, these fluctuations are comparatively small to other changes that have occurred in the basin.

5.4 Paleolacustrine history

The sediments from the Mababe Depression in this study can be interpreted as a record of a dynamic lacustrine system, where the lake spatial extent and depth and water chemistry have changed several times in the preceding ~64,000 years. Overall, the variations in the sediment record indicate the persistence of a large, stable relatively deep body of water. The lake was fresh between sedimentation from 560 and 400 cm, 380 to 325 cm, 175 to145 cm sediment depths (Fig. 4 and Fig. 5). The freshwater lake event between 560 and 400 cm depth is associated with a period of beach ridge building that ceases at about 60 ka (Fig. 11) (Burrough and Thomas, 2009). The beach ridge records the interval of ridge duration but the data from this study indicates the high lake levels are temporally more extensive. The freshwater lake event between 380 and 325 cm depths is OSL dated to begin at 41.31 ka and corresponds to high lake levels found in other studies in northwestern Botswana. A similar interval is recognized in the Makgadikgadi Pans and Lake Ngami. Ringrose et al. (2007) report a paleolake event from >41-43 ka, and Huntsmann-Mapila et al. (2006) reports lacustrine conditions from 42 ka until ca. 40 ka. This is also in agreement with earlier ages from ^{14}C dating that gave high lake levels in Makgadikgadi at this time interval (Cooke and Verstappen; 1984, Shaw and Thomas; 1988; Thomas and Shaw, 1993).

Below 200 cm sedimentation depths, there is evidence for a long-term (~30,000 years) drying of the lake. During deposition of Unit 3, a major event occurred that led to the deposition of Ca, Mg, HCO_3, C_{inorg}, and $P_{mineral}$ in concentrations much greater than elsewhere in the sediment record (Fig. 3, Fig. 4, and Fig. 5). This is thought to be the result of increased erosion in the catchment due to a locally wet climate and tectonic activity that may have increased erosion in the local river catchment. When compared to paleo-mega

lake stages identified by Burrough and Thomas (2009) (Fig. 11) this event is not recognized as a time interval of high lake levels, but instead corresponds to a period of calcrete deposition. The increase in P concentrations between 290 and 190 cm depths suggest that this interval is a period of increased inflow of water into Paleolake Mababe; however, the lack of correspondence to the beach ridge records suggest that water levels did not increase enough to aggrade the beach ridges.

Amid this large influx in solute material to the basin, there appears to be a shift in the Paleolake productivity. The lower 260 cm of the lacustrine record is dominated by the productivity of diatoms, but in the upper 260 cm, diatom productivity overall declines while organic matter concentrations generally increase (Fig. 7). It is evident that a significant shift occurred in the lake above 260 cm that resulted in the slow dessication of the lake. The increased abundance of organic matter and decreased diatom accumulations indicate that the lake was shallowing possibly a result of increased outflow. If tectonic events tilted the basin to the south, as suggested by the variation in the elevation of the Magikwe Ridge (Burrough and Thomas, 2008), then when water levels rose above the 927 m asl level, it would flow out of the Mababe Depression along the Mababe River.

A deepening of Paleolake Mababe is interpreted from the productivity data between 145 cm and 120 cm sediment depths (Fig. 7). An OSL date at 135 cm (Fig. 3) gives an age in this interval of 26.96 ka. This date corresponds to high lake water conditions in Tsodilo Hills located to the northeast of the Okavango Delta (Thomas et al., 2003). The presence of a lake in the Tsodilo Hills is evidence of a locally wet climate, because the lake is not fed by any outside water source (Thomas et al., 2003). The record from Tsodilo Hills suggests that the local wet clime prevailed from 27 to 12 ka with a possible drying at 22-19 ka associated with the Last Glacial Maximum (Thomas et al., 2003). The event may also correlate with the paleo-mega lake identified by Burrough and Thomas (2009) that occurs between 20 and 30 ka (Fig. 11).

CHAPTER 6

CONCLUSIONS

The sediment record from trench MABX provides information on the biogeochemical evolution of Paleolake Mababe. Variation in proxies like pH, sediment electrical conductivity, ion concentration, opaline silica, C_{org}, C:N ratios, and $\delta^{13}C_{org}$ can be used to infer changes in water balance, which is controlled by both climate and tectonic events. The sediment record extends to ~ 65,000 years ago and includes multiple intervals with significant diatom accumulation that suggests water levels were stable for long periods of time. There is a shift in the sediment record between 260 cm and 240 cm depth. Prior to this interval, Paleolake Mababe is thought to be a large stable lake. This interval marks a destabilization of the lake that led to the eventual dessication of Paleolake Mababe in the upper 15 cm of the lithologic record. The explanation provided for the destabilization of the lake is renewed tectonic activity in the region that alters the basin morphology of the Mababe Depression.

The sediment leachate data suggests that evaporite minerals were deposited in the Paleolake Mababe sediments as a result of increased solute concentration from evaporative concentration. Evaporative concentration was enhanced in Paleolake Mababe by increasing the solute load of the source water through the erosion of calcretes in the local watersheds. $Ca(HCO_3)_2$ is the main mineral phase of the evaporative concentration of the lake water and the absence of Na, K, SO_4, and Cl mineral phases suggest that the lake was not saturated to the late stages of brine development until the last 15 cm in the sediment record. Deposition of an anomalously high carbonate in the sediment record along with increases in the concentration of P at 390 cm and between 290 cm and 240 cm, 220 cm, and 120 cm depths suggest that the high concentrations of Ca in the sediment at these intervals is not solely the result of evaporative concentration. During this time period Ca is transported into the Paleolake from local watershed erosion.

The lacustrine bioproductivity data indicates that diatoms growth was dependent on the availability of nutrients especially the availability of P. The diatoms begin to decline in the upper 240 cm of the sediment record and are not tied to a decline in nutrient availability, suggesting that the diatoms concentration decreases as a result of a decrease in the water depth. In the upper 240 cm of the sediment record, diatom growth does increase between 145 cm and 120 cm around 27 ka and corresponds to an increase in lake water level.

The organic matter does not begin to accumulate in Paleolake Mababe in significant amounts until the upper 260 cm of the sedimentary record. This increase in the organic matter productivity is attributed to shallower lake conditions that led to the development of marsh/wetland vegetation. The development of the Okavango Delta could also provide a source for increased supply of organics into the Mababe Depression. Higher percent of organic matter from vascular vegetation was entering Paleolake Mababe in the upper 260 cm because of the development of wetland/marsh conditions and this is recorded in the increase in C:N ratios. An increase does not have to be indicative of shallow conditions only. This is seen in sediments between 260 cm and 210 cm depths where it is suggested that a large quantity of the organic matter is being delivered to Paleolake Mababe from the watersheds. The $\delta^{13}C_{org}$ data indicates that during the time period of sedimentation below 260 cm, there was overall a steady shift to more negative values in the $\delta^{13}C_{org}$ indicating aquatic conditions. Above sedimentation depths of 260 cm, the $\delta^{13}C_{org}$ begins to fluctuate as the water levels fluctuate and submerged and emergent wetland vegetation becomes more significant, due to fluctuating climate conditions.

CHAPTER 7

FUTURE RESEARCH

The study area is uniquely suited for investigating lithospheric/surface interactions and how these interactions alter the hydrology of a region. To understand the control that tectonics has on the surface processes of northwest Botswana a better understanding of the ORZ Rift is needed. Also, more research is necessary to understand the role that natural climate variations has had on the region. The Mababe Depression and other paleolake basins in the region remain a prime location to further the research into the paleo-hydrology and paleo-climate of northwestern Botswana.

Future research investigating the diatom communities in the Mababe Depression would provide valuable information about paleolimnological conditions. The abundance, preservation, and sensitivity of diatom species to variations in their environment make diatom taxa studies ideal indicators of minor changes in paleolake conditions (Bradbury, 1986; Smol and Cumming, 2000). Diatom taxa may indicate minor changes in Paleolake Mababe not resolved in the current study. Diatoms are abundant in the sediments collected from the Mababe Depression creating an ideal study location for diatom communities. The study looking at the diatom speciation would provide a more definitive understanding of the paleolake levels and possibly provide confirmation of a drastic change in water depth. A diatom community study would also provide information on changes in pH, water salinity, and trace metal concentrations (Reed, 1998; Peinerud et al., 2000). This information could be used to confirm the sediment leach analysis from the current research and the trace metal analysis from Gamrod (2009). Diatoms in sediment from trench MABX and elsewhere in the Mababe Depression provide the key to reconciling the water depths and lake conditions of Paleolake Mababe.

Even with a more complete understanding of the paleolake levels from diatom communities it is imperative to further constrain the timing of events in Paleolake Mababe by increasing the number of age dates for Trench MABX. ^{14}C

dates on bulk organic material in the sediment samples would be valuable for determining sedimentation rates in the Mababe Depression. Increasing the age constraints would make the current study easily comparable to other studies in the region. A more accurate comparison would make deciphering the influence of regional climate on the hydrology of northwestern Botswana verses possible lithospheric controls on the hydrology.

Future trenching may also prove to be valuable when investigation changes in the hydrology of northern Botswana. Trench MABX currently is located in the southwestern portion of the Depression near the Mababe River and Mababe swamp. The current location likely records sediment influx and changes that occurred locally in this part of the Depression. Trenches further to the north near the Savuti swamp and Ngwezumba Delta would provide information on the influence of the Linyanti River and local precipitation and drainage from the west along the Ngwezumba River.

REFERENCES

Anderson, L.D., Delaney, M.L., 2000. Sequential extraction and analysis of phosphorus in marine sediments: streamlining of theSEDEX procedures. Limnology and Oceanography 45, 509-515.

Andersson, L., Martin, J.W., Todd, C., Hughes, D.A., Earle, A., Kniveton, D., Layberry, R., Savenije, H.H.G., 2006, Impact of climate change and development scenarios on flow patterns in the Okavango River. Journal of Hydrology 331, 43-57.

Platt, B.J., 1988. Fossil diatoms and Neogene paleolimnology. Palaeogeography, Palaeoclimatology, Palaeoecology 62, 299-316.

Beuning, K.R.M., Talbot, M.R., Livingstone, D.A., Schmukler, G., 2003. Sensitivity of carbon isotopic proxies to paleoclimatic forcing: A case study from lake Bosumtwi, Ghana, over the last 32,000 years. Global Biogeochemical Cycles 17, 1121.

Burrough, S.L., and Thomas, D.S.G., 2009. Geomorphological contributions to palaeolimnology on the African continent. Geomorphology 103, 285-298.

Burrough, S.L., and Thomas, D.S.G., 2008. Late Quaternary lake-level fluctuations in the Mababe Depression: Middle Kalahari palaeolakes and the role of Zambezi inflows. Quaternary Research 69, 388-403.

Burrough, S.L., Thomas, D.S.G., Shaw, P.A., and Bailey, R.M., 2007. Multiphase quaternary highstands at lake Ngami, Kalahari, northern Botswana. Palaeogeography Palaeoclimatology Palaeoecology 253, 280-299.

Cooke, H.J., and Verstappen, H.T., 1984. The Landforms of the western Makgadikgadi Basin in Northern Botswana, with a consideration of the chronology of the evolution of Lake Palaeo-Makgadikgadi. Zeitschrift Fur Geomorphologie 28, 1-19.

Cooke, H.J., 1979. Landform evolution in the context of climatic change and neo-tectonism in the Middle Kalahari of north-central Botswana. Transactions of the Institute of British Geograpers 5, 80-99.

De Vogel, S.B., Magee, J.W., Manley, W.F., Miller, G.H., 2004. A GIS-based reconstruction of late Quatemaryaphy, paleohydrology: Lake Eyre, arid central Australia. Palaeogeography, Palaeoclimatology, Plaeoecology 204, 1-13.

Du Toit, A.L., 1926, Report on the Kalahari reconnaissance of 1925. Dept. of Irrigation, Pretoria.

Eckardt, F.D., Bryant, R.G., McCulloch, G., Spiro, B., Wood, W.W., 2008. The hydrochemistry of a semi-arid pan basin case study: Sua Pan, Makgakikgadi, Botswana. Applied Geochemistry 23, 1563-1580.

Eugster, H.P., and Jones, B.F., 1979a. Behavior of major solutes during closed-basin brine evolution. American Journal of Science 279, 609-631.

Eugster, H.P., Maglione, G., 1979b. Brines and evaporates of the Lake Chad basin, Africa. Geochimica et Cosmochimica Acta 43, 973-981.

Gamrod, J. L., 2009. Paleolimnological records of environmental change in Paleolake Mababe, Northwest Botswana. M.S. Thesis, Oklahoma State University, 121 pg.

Grey, D.R.C., and Cooke, H.J., 1977. Some problems in the quaternary evolution of the landforms in northern Botswana. Catena 4, 123-133.

Grove, A.T., 1969. Landforms and climatic change in Kalahari and Ngamiland. Geographical Journal 135, 191-212.

Gumbricht, T., McCarthy, T.S., and Merry, C.L., 2001. The topography of the Okavango Delta, Botswana, and its tectonic and sedimentological implications. South African Journal of Geology 104, 243-264.

Hach Company, 1992. Water analysis handbook, Hach Company, Loveland, Co.

Haddon, I.G., McCarthy, T.S., 2005. The Mesozoic-Cenozoic interior sag basins of Central Africa: The Late-Cretaceous-Cenozoic Kalahari and Okavango basins. Journal of African Earth Sciences 43, 316-333

Huntsman-Mapila, P., Ringrose, S., Mackay, A.W., Downey, W.S., Modisi, M., Coetzee, S.H., Tiercelin, J.J., Kampunzu, A.B., and Vanderpost, C., 2006. Use of the geochemical and biological sedimentary record in establishing palaeo-environments and climate change in the Lake Ngami basin, NW Botswana. Quaternary International 148, 51-64.

Jannerjahn, T. C., Knoppers, B.A., de Souza, W.F.L., Brunskill, G.J., Ivan, E., Silva, L., Adi, S., 2006. Factors controlling dissolved silica in tropical rivers. In. Ittekkot, v., Unger, D., Humborg, C., Tac An, N. (Eds.), The Silicon Cycle. Island Press, Washington D.C., pp. 29-51.

Kampunzu, A.B., Ringrose, S., Huntsman-Mapila, P., Harris, C., Vink, B.W., Matheson, W., 2007. Origins and palaeo-environments of Kalahari duricrusts in the Moshaweng dry valleys (Botswana) as detected by major and trace element composition. Journal of African Earth Sciences 48, 199-221.

Kgathi DL, Kniveton D, Ringrose S, Turton AR, Vanderpost CHM, Lundqvist J, Seely M. 2006, The Okavango; a river supporting its people, environment and economic development. Journal of Hydrology 331, 3-17.

Krishnamurthy, R.V., Syrup, K. Long, A., 1999. Is selective preservation of nitrogenous organic matter reflected in the $\delta^{13}C$ signal of lacustrine sediments? Chemical Geology 158, 165-172.

Kroger , M., Lorenz, S., Brunner, E., Sumper, M., 2002. Self-assembly of highly phosphorylated silaffins and their function in biosilica morphogenesis. Science 298, 584-586.

Latimer, C.J., Filippelli, G.M., Hendy, I., Newkirk, D.R., 2006. Opal-associated particulate phosphorus: Implications for the marine P cycle. Geochimica et Comochimimica Acta 70, 3843-3854.

Lent, R.M., Lyons, W.B., Showers, W.J., Johannesson, K.H., 1995. Late Holocene paleoclimatic and paleobiologic records from sediments of Devils Lake, North Dakota. Journal of Paleolimnology 13, 193-207.

McCarthy, T.S., and Metcalfe, J., 1990. Chemical sedimentation in the semi-arid environment of the Okavango Delta, Botswana. Chemical Geology 89, 157-178.

McCarthy , T.S., and Ellery, W.N., 1995. Sedimentation of the distal reaches of the Okavango Fan, Botswana, and its bearing on clacrete and silcrete (Ganister) formation. Journal of Sedimentary Research A65, 77-90.

McCarthy, T.S., and Ellery, W.N., 1998. The Okavango Delta. Transactions of the Royal Society of South Africa 53, 157-182.

McCarthy, T.S., Smith, N.D., Ellery, W.N., Gumbricht, T., 2002. The Okavango Delta-Semiarid alluvial-fan sedimentation related to incipient rifting. SEPM Special Publication 73, 179-193.

Meyers, P. A., Ishiwatari, R., 1993. Lacustrine organic geochemistry an overview of indicators of organic matter sources and diagenesis in lake sediments. Organic Geochemistry 20, 867-900.

Milzow, C., Kgotlhang, L., Bauer-Gottwein, P., Meier, P., Kinzelbach, W., 2009. Regional review: the hydrology of the Okavango Delta Botswana – processes, data and modelling. Hydrogeology Journal 17, 1297-1328.

Mladenov, N., McKnight, D.M., Macko, S.A., Norris, M, Cory, R.M., Ramberg, L., 2007. Chemical characterization of DOM in channels of a seasonal wetland, Aquatic Science 69, 456-471.

Modisi, M.P., Atekwana, E.A., Kampunzu, A.B., Ngwisanyi, T.H., 2000. Rift Kinematics during the incipient stages of continental extension. Evidence from the nascent Okavango rift basin, northwest Botswana. Geology 28, 939-942.

Mortlock, R.A., Froelich, P.N., 1989. A simple method for the rapid determination of biogenic opal in pelagic marine sediments. Deep-Sea Research 36, 1415-1426.

Muzuka, A.N.N., Ryner, M., Holmgren, K., 2004. 12,000-Year, preliminary results of the stable nitrogen and carbon isotope record from the Empakai Crater lake sediments, Northern Tanzania. Journal of African Earth Sciences 40, 293-303.

Murray, A.S., Wintle, A.G., 2008. Luminescence dating quartz using an improved single aliquot regenerative dose protocol. Radiation Measurements 32, 57-73.

Nash, D.J., 1997. Groundwater as a geomorphological agent in drylands. Arid Zone Geomorphology: Process, Form and Change in Drylands, 2nd edition. Thomas, S.G. (Eds), John Wiley & Sons Ltd. pp. 319.

O'Leary, M.H., 1981. Carbon isotope fractionation in plants. Phytochemistry 20, 553-567

Otvos, E.G., 2000. Beach ridges—definitions and significance. Geomorphology, 32, 83–108.

Passarge, S., 1904. Die Kalahari: Berlin, Dietrich Riemer.

Peinerud, E.K., Ingri J., Ponter C, 2001. Non-detrital Si concentrations as an estimate of diatom concentrations in lake sediments and suspended material. Chemical Geology 177, 229-239.

Reed, J.M., 1998. Diatom preservation in the recent sediment record of Spanish saline lakes: implications for palaeoclimate study. Journal of Paleolimnology 19, 129-137.

Ringrose, S., Huntsman-Mapila, P., Kampunzu, A.B., Downey, W., Coetzee, S., Vink, B., Matheson, W., and Vanderpost, C., 2005. Sedimentological and

geochemical evidence for palaeo-environmental change in the Makgadikgadi subbasin, in relation to the MOZ rift depression, Botswana. Palaeogeography Palaeoclimatology Palaeoecology 217, 265-287.

Ringrose S., Huntsman-Mapila P., Downey, W., Coetzee, S., Fey, M., Vanderpost, C., Vink, B., Kemosidile, T., Dikitso, K., 2008. Diagenesis in Okavango fan and adjacent dune deposits with implications for the record of palaeo-environmental change in Makgadikgadi-Okavango-Zambezi basin, northern Botswana. Geomorphology 101, 544-557.

Ruttenberg, K.C., 1992. Development of a sequential extraction method for different forms of phosphorus in marine sediments. Liminology and Oceanography 37, 1460-1482.

Shaw, P., 1985. Late Quaternary landforms and environmental-change in northwest Botswana - the evidence of Lake Ngami and the Mababe Depression. Transactions of the Institute of British Geographers 10, 333-346.

Shaw, P., 1986. The palaeohydrology of the Okavango Delta some preliminary results. Paleoecology of Africa 17, 51-58.

Shaw, P., 1988. After the Flood - the fluvio-lacustrine landforms of Northern Botswana. Earth-Science Reviews 25, 449-456.

Smol, J. P., Cumming, B. F., 2000. Tracking long-term changes in climate using algal indicators in lake sediments. Journal of Phycology 36, 986-1011.

Sonnefeld, P., 1984. Brines and evaporates. Academic Press, Inc., Orlando, 613 pp.

Thoms, D.S.G., and Shaw, P.A., 1991. The Kalahari environment. Cambridge University Press, Cambridge, 284 pp.

Thomas, D.S.G., and Shaw, P.A., 1993. The evolution and characteristics of the Kalahari, southern Africa. Journal of Arid Environments 25, 97-108.

Thomas, D.S.G., Brook, G., Shaw, P., Bateman, M., Appleton, C., Nash, D., McLaren, S., and Davies, F., 2003. Late Pleistocene wetting and drying in the NW Kalahari: an integrated study from the Tsodilo Hills, Botswana Quaternary International 104, 53-67.

Wang, L., D'Odorico, P., Ringrose, S., Coetzee, S., Macko, S.A., 2005. Biogeochemistry of Kalahari sands. Journal of Arid Environments 71, 259-279.

Wetzel, R.G., 2001. Limnology Lake and River Ecosystems. Academic Press, San Diego, 3rd, 1006 pp.

Wintle A.G., Murray A.S., 2006. A review of quartz optically stimulated luminescence characteristics and their relevance in single-aliquot regeneration dating protocols. Radiation Measurements 41, 369-391.

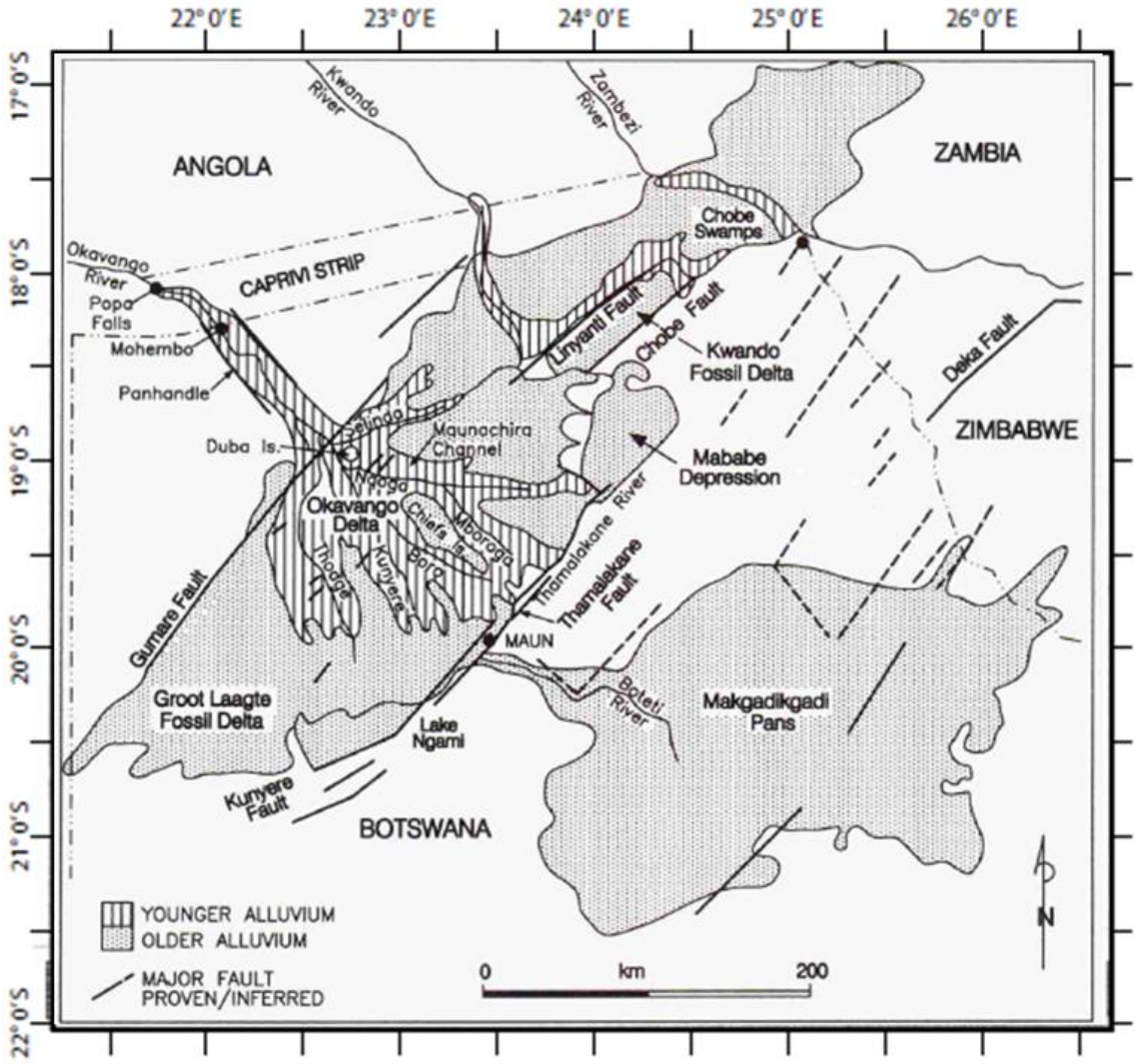

Fig. 1. Map of northwestern Botswana showing the location of the study area (Mababe Depression), and the other features of the region. (Modified from Gumbricht et al., 2001)

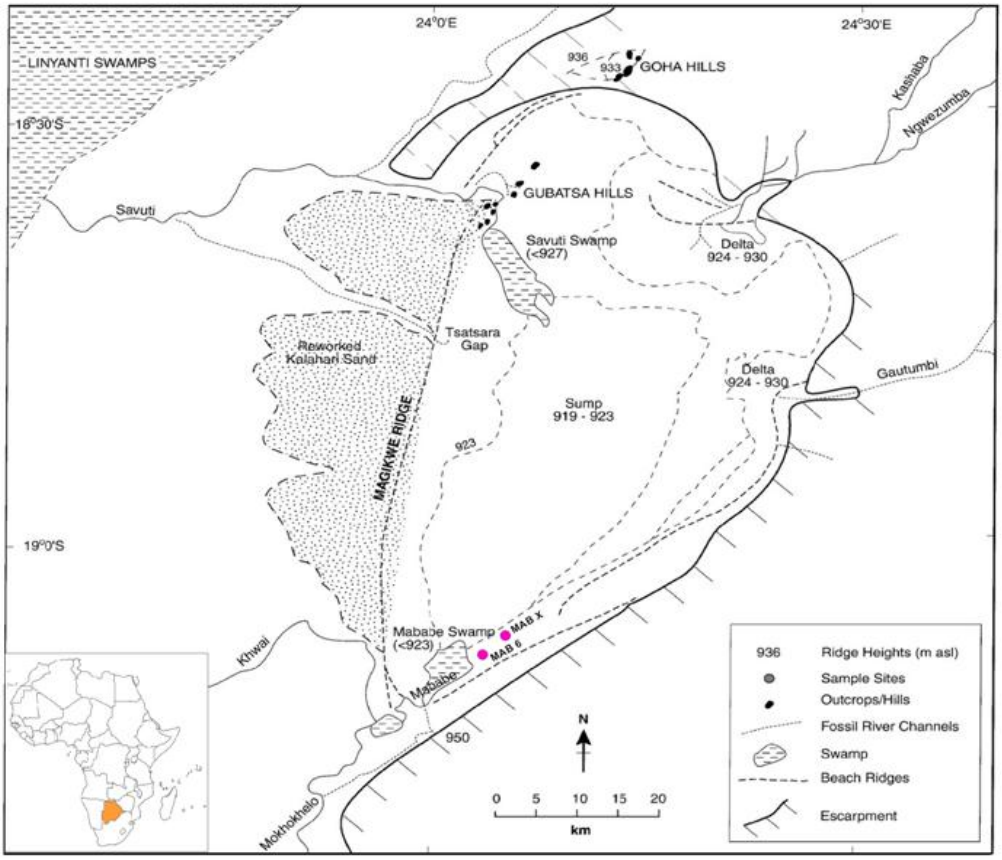

Fig. 2. Map of the Mababe Depression, northwestern, Botswana. Trench location of MABX is indicated by filled circle (Modified from Burrough and Thomas, 2007).

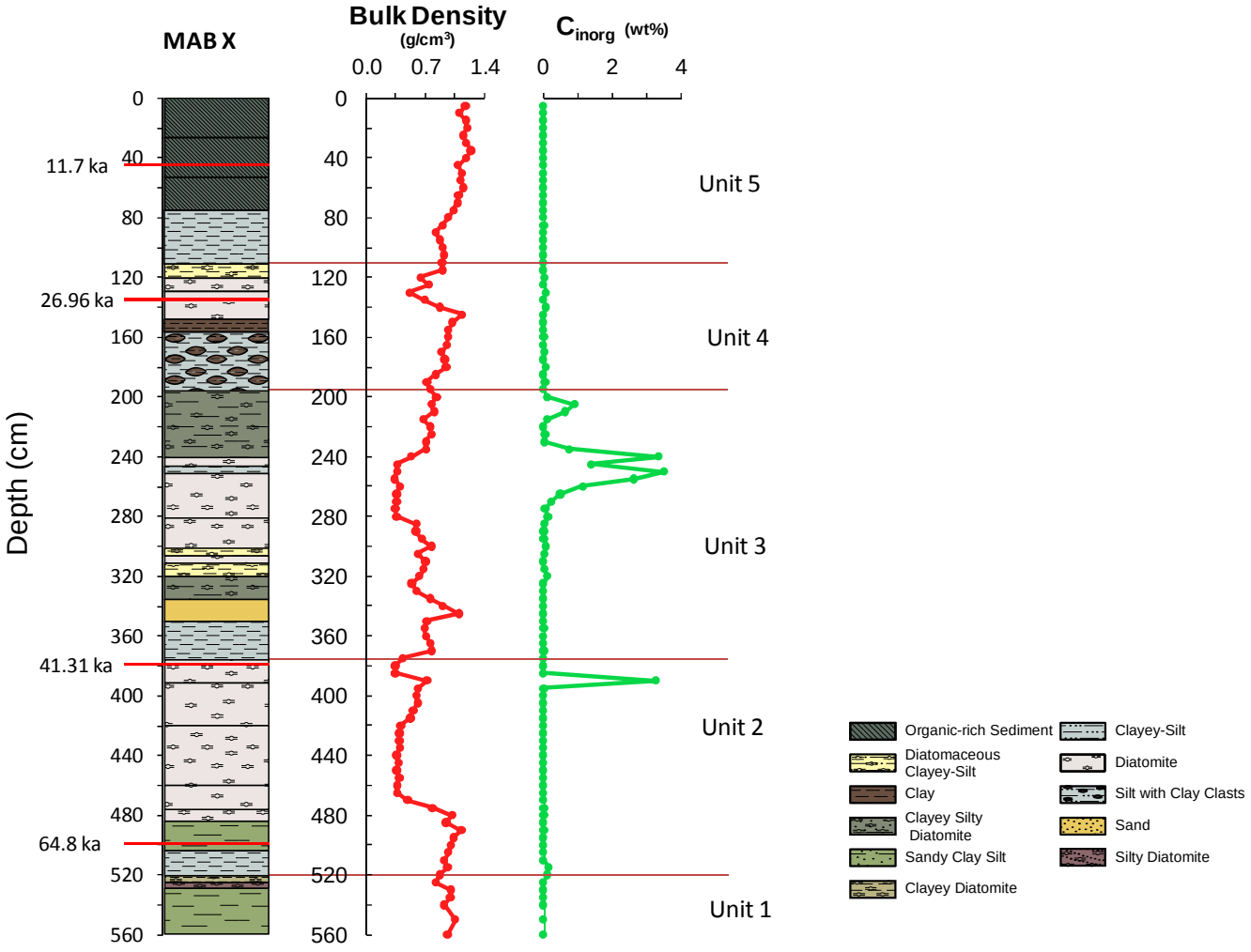

Fig. 3. Lithologic section of MABX depicting units sampled in the trench. Also shows the depth variation in the bulk density and inorganic carbon (C_{inorg}) concentration.

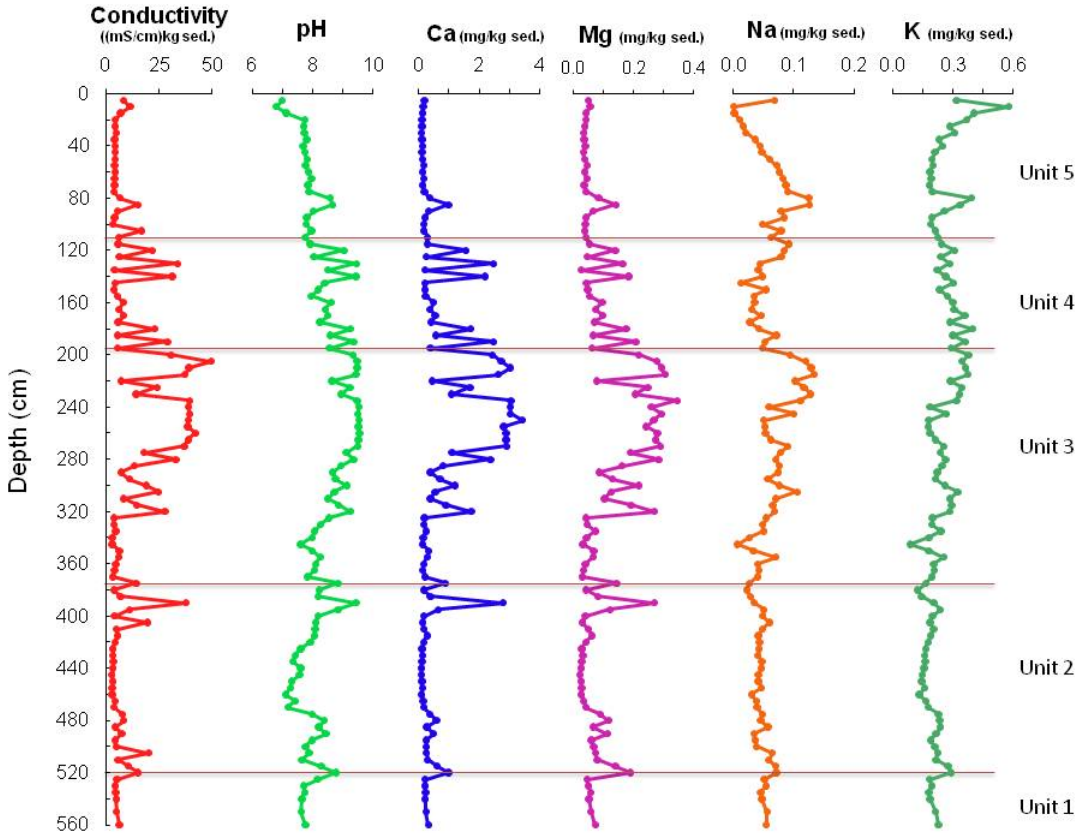

Fig. 4. Depth variation in the electrical conductivity, pH, Ca, Mg, Na, and K from sediment leachate from the MABX trench.

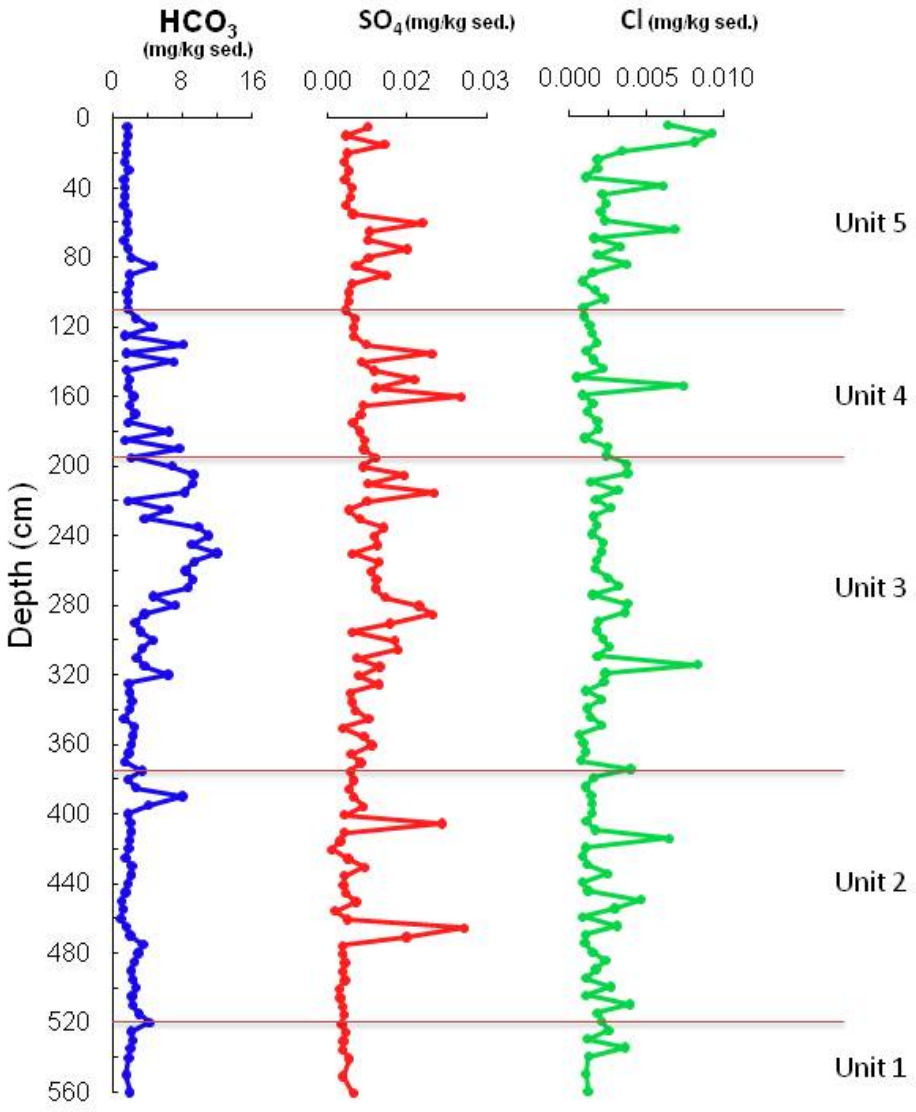

Fig. 5. Depth variation in HCO_3, SO_4, and Cl concentrations of the sediment leachate from the MABX trench.

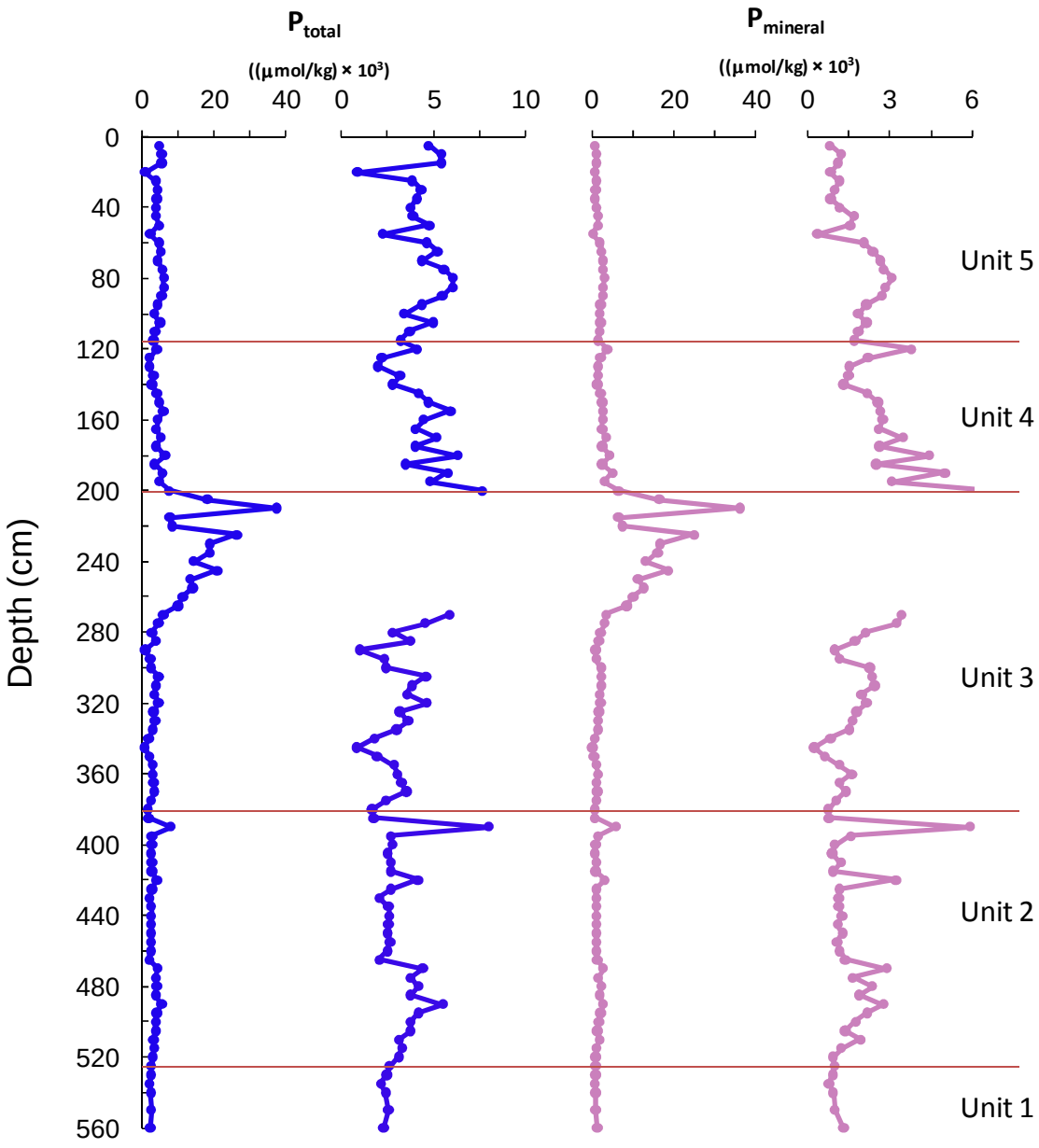

Fig. 6. Depth variation in total phosphorus (P_{total}) and mineral phosphorus ($P_{mineral}$) in sediments from the MABX trench.

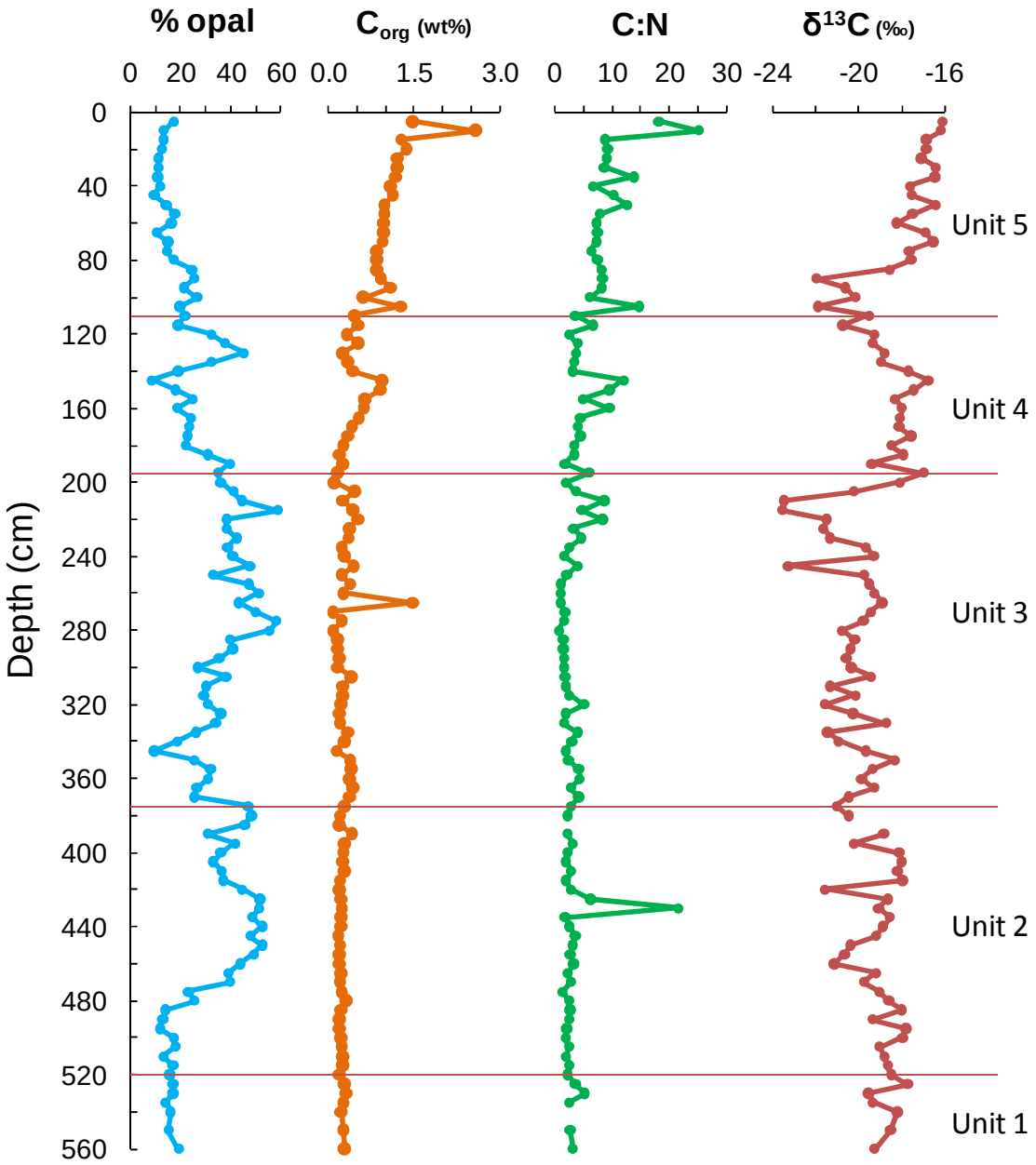

Fig. 7. Depth variation in biogenic silica (expressed as % opal), weight % organic carbon (C_{org}), carbon to nitrogen ratios (C:N), and the stable carbon isotope ratio of bulk organic matter ($\delta^{13}C_{org}$) in sediments from MABX trench.

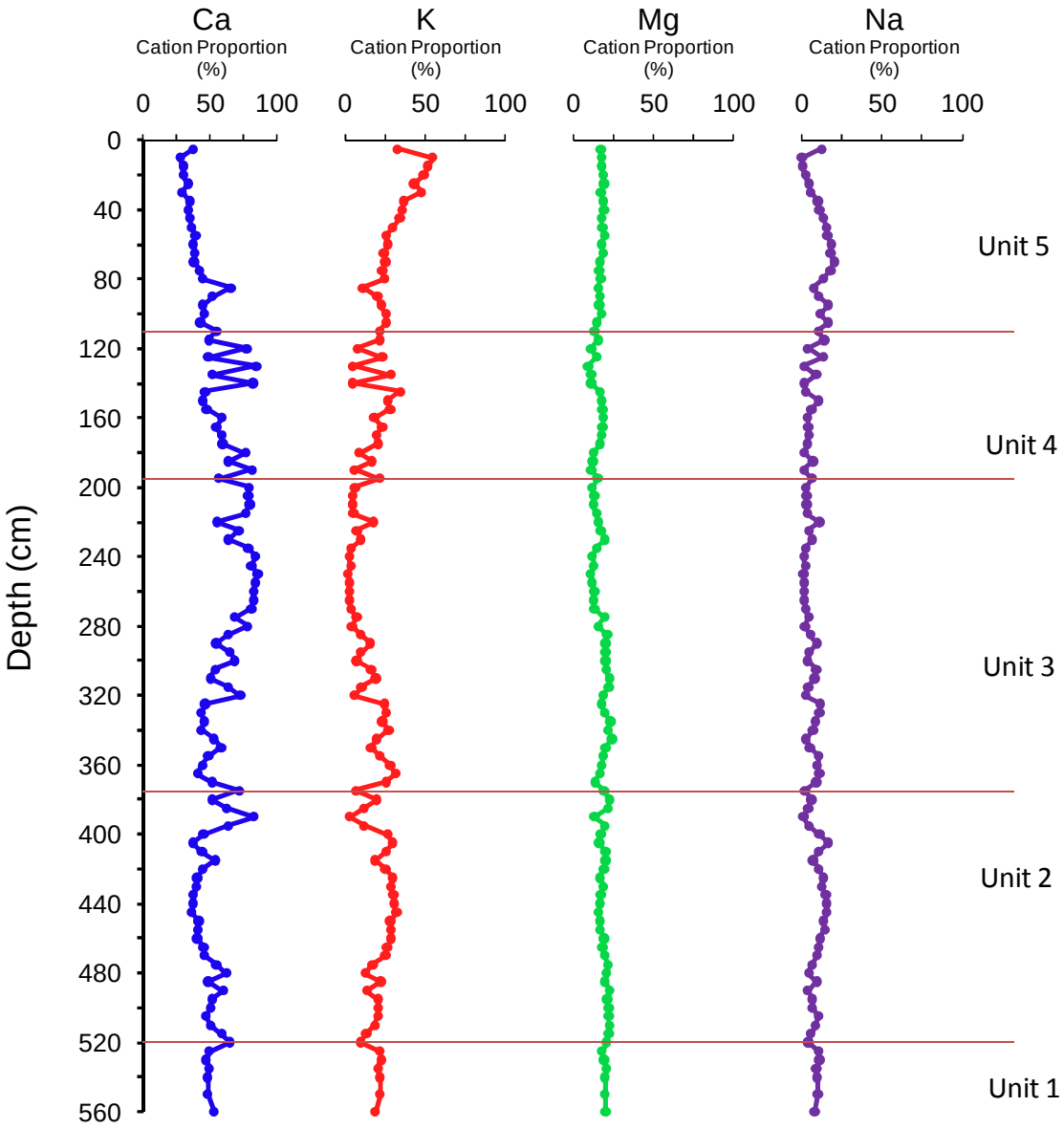

Fig. 8. Depth variation in the proportions of Ca, K, Mg, and Na from sediment leachate from the MABX trench.

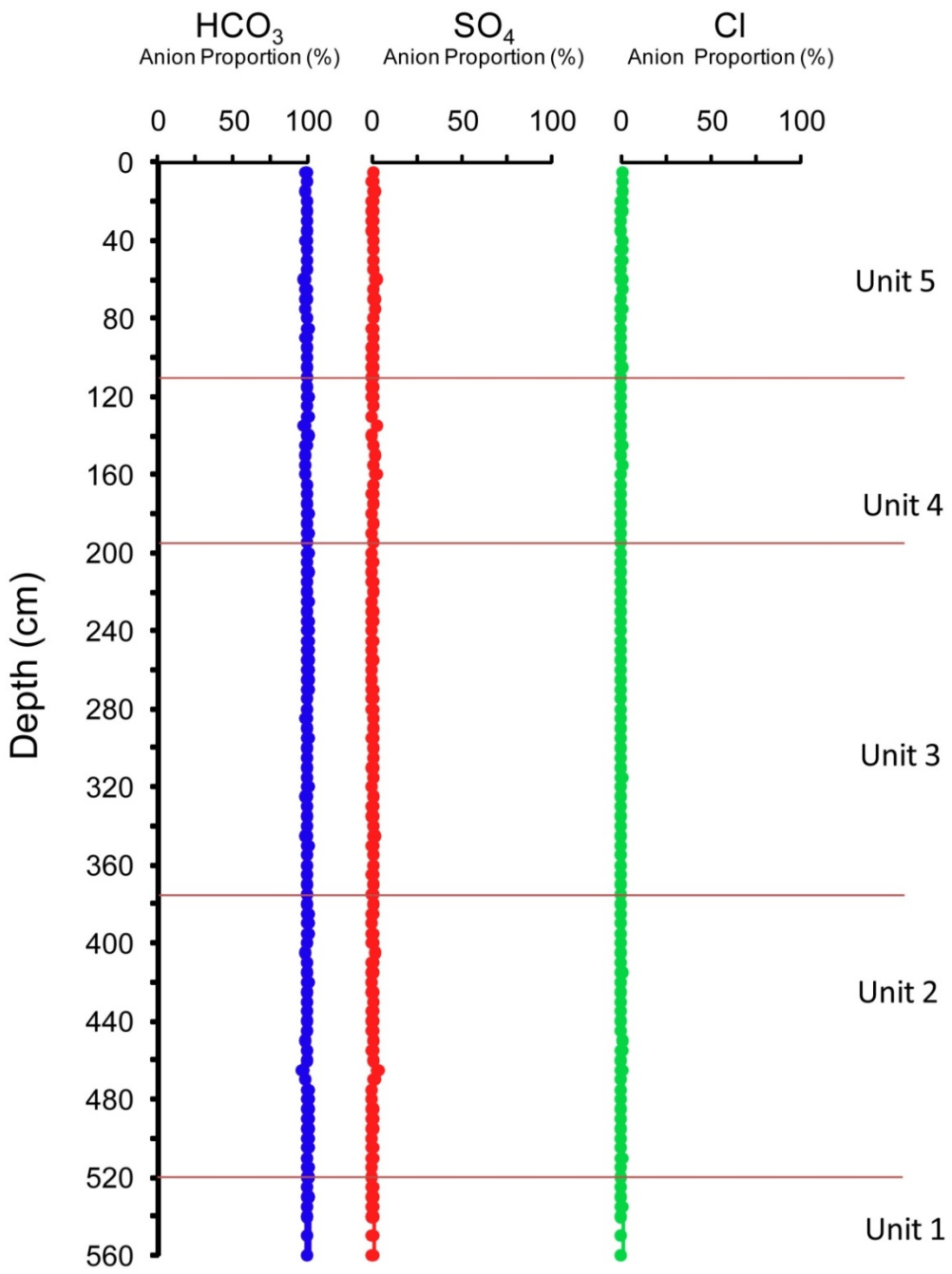

Fig. 9. Depth variation in the proportions of HCO_3, SO_4, and Cl of sediment leachate from the MABX trench.

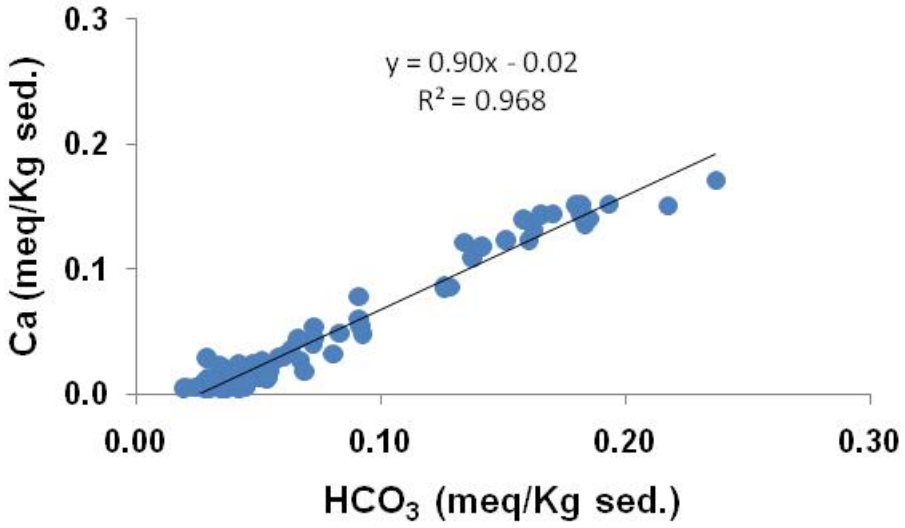

Fig. 10. Crossplot of Ca vs. HCO_3 from sediment leachate from the MABX trench.

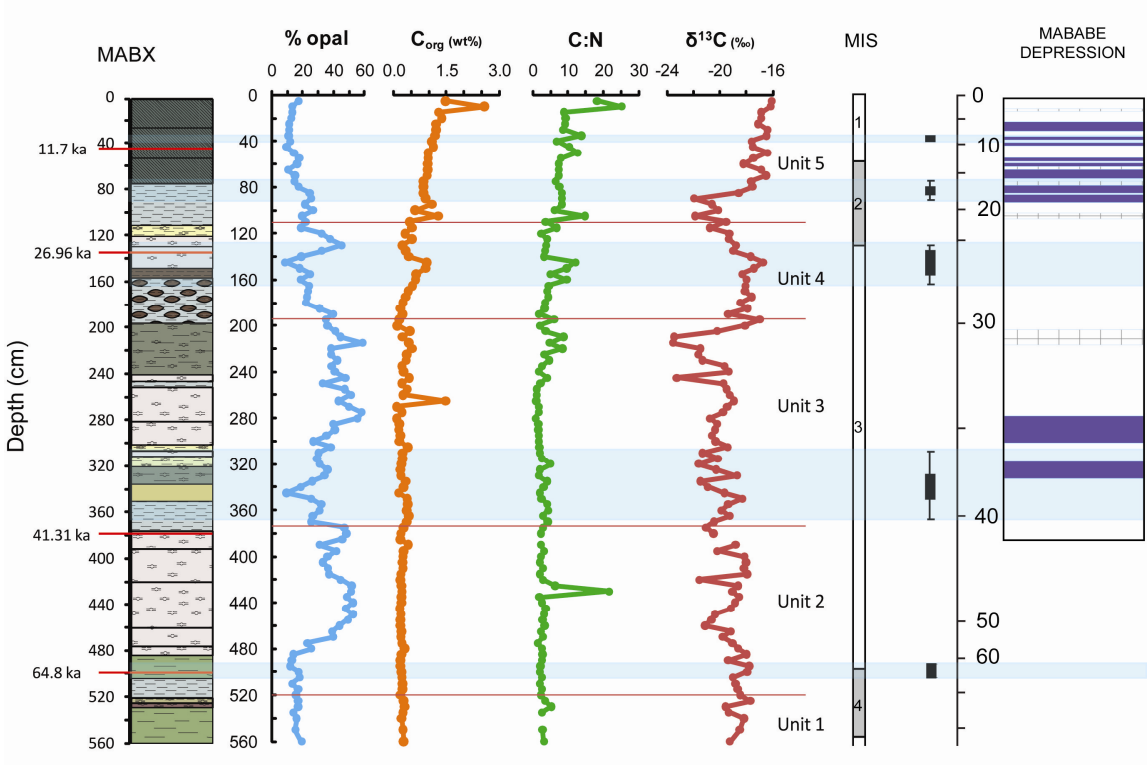

Fig. 11. Depth variation in % opal, C_{org}, $\delta^{13}C$, and C:N ratios along with the marine isotope stages (MIS) and high lake stands in the Mababe Depression. Inferred paleo-mega lake stages are depicted as blue bars across the graph. The record for the Mababe Depression from beach ridge chronologies is illustrated with purple bars indicating high lake levels and hatched bars indicating calcrete formation (modified from Burrough and Thomas, 2009).

APPENDIX

A1

Depth cm	Munsel Color I.D.	Munsel Color Description
5	7.5YR4/1	dark gray
10	7.5YR4/1	dark gray
15	10YR4/1	dark gray
20	10YR4/1	dark gray
25	10YR4/1	dark gray
30	10YR4/1	dark gray
35	10YR4/1	dark gray
40	10YR4/1	dark gray
45	10YR4/1	dark gray
50	10YR4/1	dark gray
55	10YR4/1	dark gray
60	10YR4/1	dark gray
65	10YR4/1	dark gray
70	10YR4/1	dark gray
75	10YR4/1	dark gray
80	10YR5/1	gray
85	10YR5/1	gray
90	10YR5/1	gray
95	10YR5/1	gray
100	10YR5/1	gray
105	10YR5/1	gray
110	10YR5/1	gray
115	10YR5/1	gray
120	2.5YR7/1	light gray
125	2.5YR7/1	light gray
130	2.5YR7/1	light gray
135	2.5YR7/1	light gray
140	2.5YR7/1	light gray
145	10YR4/1	dark gray
150	10YR4/1	dark gray
155	10YR5/1	gray
160	10YR5/1	gray
165	2.5YR6/1	gray
170	2.5YR5/1	gray
175	2.5YR6/1	gray
180	2.5YR6/1	gray
185	2.5YR7/1	light gray
190	2.5YR7/1	light gray
195	2.5YR7/1	light gray
200	2.5YR7/1	light gray
205	2.5YR7/1	light gray
210	2.5YR7/1	light gray
215	2.5YR7/1	light gray
220	2.5YR6/2	light brownish gray
225	2.5YR6/2	light brownish gray
230	2.5YR6/2	light brownish gray
235	2.5YR7/2	light gray

Depth cm	Munsel Color I.D.	Munsel Color Description
240	2.5YR7/2	light gray
245	2.5YR8/1	white
250	2.5YR7/2	light gray
255	2.5YR8/1	white
260	2.5YR8/1	white
265	2.5YR8/1	white
270	2.5YR8/1	white
275	2.5YR8/1	white
280	2.5YR8/1	white
285	2.5YR7/2	light gray
290	2.5YR7/2	light gray
295	2.5YR7/2	light gray
300	2.5YR7/2	light gray
305	2.5YR6/2	light brownish gray
310	2.5YR7/2	light gray
315	2.5YR7/2	light gray
320	2.5YR7/2	light gray
325	2.5YR7/2	light gray
330	2.5YR7/2	light gray
335	2.5YR7/1	light gray
340	2.5YR6/2	light brownish gray
345	2.5YR6/2	light brownish gray
350	2.5YR6/2	light brownish gray
355	2.5YR6/2	light brownish gray
360	2.5YR6/2	light brownish gray
365	2.5YR6/2	light brownish gray
370	2.5YR6/2	light brownish gray
375	2.5YR6/2	light brownish gray
380	2.5YR8/1	white
385	2.5YR8/1	white
390	2.5YR8/1	white
395	2.5YR7/2	light gray
400	2.5YR7/2	light gray
405	2.5YR7/2	light gray
410	2.5YR7/2	light gray
415	2.5YR7/2	light gray
420	2.5YR8/1	white
425	2.5YR8/1	white
430	2.5YR8/1	white
435	2.5YR8/1	white
440	2.5YR8/1	white
445	2.5YR8/1	white
450	2.5YR8/1	white
455	2.5YR8/1	white
460	2.5YR8/1	white
465	2.5YR8/1	white
470	2.5YR7/1	light gray

Depth cm	Munsel Color I.D.	Munsel Color Description
475	2.5YR7/2	light gray
480	2.5YR6/2	light brownish gray
485	2.5YR6/2	light brownish gray
490	2.5YR6/2	light brownish gray
495	2.5YR6/2	light brownish gray
500	2.5YR6/2	light brownish gray
505	2.5YR6/2	light brownish gray
510	2.5YR6/2	light brownish gray
515	2.5YR6/2	light brownish gray
520	2.5YR6/2	light brownish gray
525	2.5YR6/1	gray
530	2.5YR6/2	light brownish gray
535	2.5YR6/2	light brownish gray
540	2.5YR6/2	light brownish gray
545	2.5YR6/2	light brownish gray
550	2.5YR6/2	light brownish gray
555	2.5YR6/2	light brownish gray
560	2.5YR6/2	light brownish gray

APPENDIX

A2

Depth	Dry Bulk Density	C_{inorg}	Electrical conductivity	pH	Ca	Mg	Na	K	HCO_3	Cl	SO_4
cm	g/cm^3	wt. %	(mS/cm)/kg	SU	mg/kg	mg/kg	mg/kg	mg/kg	mg/kg	mg/kg	mg/kg
5	1.17	0.002	4.0	7.00	0.184	0.052	0.069	0.317	1.685	0.006	0.008
10	1.10	0.005	5.7	6.80	0.148	0.057	0.001	0.575	1.774	0.009	0.003
15	1.18	0.002	3.4	7.13	0.120	0.044	0.002	0.404	1.600	0.008	0.011
20	1.19	0.003	2.2	7.74	0.114	0.043	0.011	0.367	1.575	0.003	0.004
25	1.15	0.000	2.1	7.70	0.113	0.039	0.016	0.284	1.399	0.002	0.003
30	1.19	0.001	2.4	7.73	0.097	0.035	0.021	0.309	1.861	0.002	0.004
35	1.23	0.002	2.1	7.81	0.113	0.037	0.036	0.230	1.341	0.001	0.003
40	1.18	0.003	2.1	7.68	0.119	0.041	0.044	0.247	1.462	0.006	0.005
45	1.09	0.010	2.2	7.74	0.109	0.034	0.048	0.211	1.443	0.002	0.004
50	1.13	0.002	2.1	7.82	0.124	0.038	0.060	0.197	1.350	0.002	0.003
55	1.12	0.001	1.9	7.77	0.157	0.047	0.072	0.200	1.733	0.002	0.005
60	1.15	0.001	2.2	7.86	0.136	0.038	0.076	0.187	1.603	0.002	0.018
65	1.09	0.000	2.1	7.97	0.158	0.047	0.083	0.193	1.796	0.007	0.008
70	1.08	0.000	1.9	7.85	0.141	0.037	0.087	0.185	1.340	0.002	0.008
75	1.03	0.002	1.8	7.89	0.187	0.043	0.091	0.199	1.781	0.003	0.015
80	0.97	0.007	3.3	8.57	0.363	0.085	0.125	0.392	2.191	0.002	0.008
85	0.90	0.020	7.6	8.67	0.976	0.142	0.126	0.335	4.713	0.004	0.005
90	0.82	0.003	2.8	8.03	0.335	0.065	0.079	0.258	2.018	0.002	0.011
95	0.88	0.001	2.1	7.81	0.197	0.043	0.084	0.194	2.022	0.001	0.005
100	0.91	0.000	1.7	7.79	0.175	0.040	0.049	0.191	1.710	0.002	0.004
105	0.92	0.002	8.4	7.97	0.180	0.038	0.079	0.213	1.740	0.002	0.004
110	0.89	0.004	3.0	7.75	0.294	0.043	0.063	0.226	1.846	0.001	0.003
115	0.90	0.006	2.9	7.92	0.286	0.054	0.092	0.244	2.748	0.001	0.005
120	0.64	0.029	11.1	9.04	1.567	0.140	0.084	0.308	4.622	0.001	0.005
125	0.74	0.002	3.1	8.04	0.256	0.047	0.080	0.240	1.481	0.001	0.005
130	0.51	0.086	16.9	9.45	2.473	0.164	0.044	0.283	8.167	0.002	0.007
135	0.69	0.004	2.1	8.49	0.206	0.027	0.041	0.223	1.568	0.001	0.020
140	0.87	0.076	15.2	9.44	2.199	0.184	0.049	0.264	7.000	0.002	0.006
145	1.13	0.001	2.2	8.40	0.208	0.045	0.013	0.303	1.624	0.002	0.009
150	1.02	0.003	1.8	8.19	0.200	0.049	0.055	0.234	1.954	0.000	0.016
155	0.97	0.004	2.7	7.95	0.233	0.054	0.034	0.272	1.762	0.007	0.009
160	0.97	0.015	3.9	8.61	0.496	0.097	0.036	0.300	2.420	0.001	0.025
165	0.96	0.010	3.0	8.42	0.371	0.074	0.030	0.306	1.945	0.002	0.007
170	0.89	0.046	4.3	8.51	0.549	0.099	0.046	0.360	2.619	0.001	0.006
175	0.93	0.002	2.9	8.24	0.419	0.070	0.028	0.283	1.842	0.002	0.005

Depth	Dry Bulk Density	C_{inorg}	Electrical conductivity	pH	Ca	Mg	Na	K	HCO_3	Cl	SO_4
cm	g/cm^3	wt. %	(mS/cm)/kg	SU	mg/kg	mg/kg	mg/kg	mg/kg	mg/kg	mg/kg	mg/kg
180	0.94	0.073	11.5	9.26	1.722	0.176	0.043	0.399	6.530	0.002	0.006
185	0.82	0.008	2.8	8.59	0.578	0.066	0.071	0.299	1.477	0.001	0.007
190	0.72	0.056	14.7	9.35	2.478	0.208	0.052	0.362	7.694	0.003	0.007
195	0.76	0.008	2.7	8.56	0.389	0.064	0.049	0.292	2.185	0.002	0.009
200	0.83	0.107	15.5	9.33	2.434	0.218	0.094	0.377	6.822	0.004	0.007
205	0.77	0.910	23.7	9.47	2.736	0.278	0.120	0.345	9.329	0.004	0.014
210	0.81	0.645	19.6	9.48	3.042	0.292	0.129	0.364	9.252	0.001	0.008
215	0.67	0.110	18.1	9.43	2.639	0.304	0.134	0.374	8.267	0.003	0.020
220	0.76	0.009	3.6	8.64	0.450	0.079	0.102	0.287	1.740	0.002	0.007
225	0.77	0.059	11.9	9.24	1.701	0.248	0.117	0.343	6.403	0.003	0.004
230	0.71	0.041	7.2	8.94	1.086	0.205	0.128	0.331	3.704	0.002	0.006
235	0.70	0.754	19.8	9.48	3.053	0.343	0.111	0.318	9.833	0.002	0.011
240	0.53	3.343	19.2	9.52	3.028	0.259	0.060	0.186	11.062	0.001	0.009
245	0.36	1.387	20.0	9.50	3.030	0.292	0.100	0.268	9.135	0.002	0.009
250	0.36	3.490	19.1	9.54	3.436	0.267	0.051	0.180	12.058	0.002	0.005
255	0.34	2.626	18.8	9.51	2.816	0.242	0.052	0.179	9.406	0.002	0.010
260	0.40	1.139	20.8	9.55	2.888	0.279	0.054	0.187	8.417	0.002	0.008
265	0.36	0.498	19.5	9.51	2.884	0.273	0.062	0.215	9.252	0.003	0.009
270	0.36	0.239	18.6	9.49	2.900	0.289	0.090	0.255	8.670	0.003	0.009
275	0.34	0.059	8.9	9.11	1.103	0.189	0.078	0.237	4.653	0.002	0.011
280	0.36	0.138	15.9	9.36	2.379	0.283	0.070	0.263	7.188	0.004	0.017
285	0.59	0.049	6.6	8.93	0.804	0.162	0.076	0.245	3.682	0.004	0.020
290	0.59	0.018	3.6	8.67	0.384	0.085	0.074	0.222	2.610	0.002	0.012
295	0.65	0.024	5.5	8.76	0.706	0.131	0.058	0.215	3.217	0.002	0.005
300	0.77	0.072	9.5	9.13	1.213	0.217	0.076	0.259	4.636	0.002	0.013
305	0.61	0.028	12.5	8.72	0.547	0.126	0.106	0.323	3.416	0.003	0.013
310	0.70	0.010	4.1	8.51	0.383	0.104	0.070	0.287	2.760	0.002	0.006
315	0.68	0.030	7.2	8.87	0.906	0.191	0.065	0.293	3.700	0.008	0.010
320	0.63	0.127	13.3	9.25	1.737	0.270	0.068	0.284	6.411	0.002	0.006
325	0.54	0.004	2.0	8.53	0.191	0.044	0.055	0.198	1.879	0.002	0.010
330	0.60	0.003	1.9	8.25	0.170	0.047	0.049	0.196	2.020	0.001	0.004
335	0.75	0.004	2.3	8.07	0.241	0.074	0.050	0.239	2.274	0.002	0.004
340	0.90	0.001	1.5	7.98	0.148	0.045	0.027	0.181	2.000	0.001	0.005
345	1.10	0.003	1.5	7.61	0.119	0.032	0.007	0.087	1.319	0.001	0.008
350	0.72	0.010	3.1	7.99	0.330	0.069	0.033	0.181	2.539	0.002	0.003
355	0.69	0.016	3.0	8.25	0.286	0.066	0.071	0.253	2.391	0.001	0.007

Depth	Dry Bulk Density	C_{inorg}	Electrical conductivity	pH	Ca	Mg	Na	K	HCO_3	Cl	SO_4
cm	g/cm^3	wt. %	(mS/cm)/kg	SU	mg/kg	mg/kg	mg/kg	mg/kg	mg/kg	mg/kg	mg/kg
360	0.71	0.008	2.3	8.10	0.165	0.041	0.041	0.205	2.180	0.001	0.008
365	0.76	0.003	2.0	8.05	0.139	0.034	0.043	0.209	1.876	0.001	0.004
370	0.78	0.013	1.7	7.83	0.200	0.032	0.040	0.195	1.427	0.001	0.006
375	0.44	0.008	7.1	8.84	0.886	0.144	0.027	0.166	3.371	0.004	0.004
380	0.34	0.007	1.8	8.21	0.165	0.043	0.023	0.124	1.826	0.002	0.005
385	0.34	0.003	3.5	8.18	0.387	0.082	0.028	0.146	2.690	0.001	0.004
390	0.71	3.245	18.3	9.44	2.799	0.269	0.035	0.204	8.064	0.001	0.005
395	0.61	0.020	5.7	8.84	0.646	0.121	0.051	0.239	4.099	0.001	0.007
400	0.59	0.003	2.1	8.18	0.174	0.040	0.049	0.199	1.751	0.001	0.003
405	0.61	0.003	9.7	8.11	0.118	0.031	0.060	0.186	2.065	0.001	0.022
410	0.56	0.006	2.5	8.08	0.180	0.050	0.048	0.204	2.124	0.002	0.003
415	0.52	0.005	2.7	8.07	0.277	0.063	0.042	0.191	1.945	0.006	0.002
420	0.41	0.003	2.1	7.92	0.159	0.041	0.043	0.176	1.878	0.001	0.001
425	0.39	0.004	1.7	7.60	0.113	0.028	0.043	0.164	1.521	0.001	0.004
430	0.39	0.005	1.7	7.42	0.116	0.033	0.041	0.162	2.268	0.001	0.007
435	0.40	0.002	1.7	7.36	0.104	0.029	0.047	0.164	2.135	0.003	0.003
440	0.36	0.002	1.6	7.61	0.097	0.026	0.046	0.157	1.757	0.001	0.003
445	0.38	0.012	1.4	7.56	0.084	0.023	0.041	0.147	1.517	0.001	0.003
450	0.36	0.001	1.7	7.30	0.110	0.027	0.041	0.146	1.054	0.005	0.005
455	0.39	0.002	1.5	7.27	0.117	0.029	0.047	0.160	1.214	0.003	0.001
460	0.37	0.001	1.5	7.10	0.094	0.027	0.030	0.132	0.990	0.001	0.004
465	0.37	0.003	2.1	7.42	0.144	0.035	0.038	0.164	1.602	0.003	0.026
470	0.49	0.003	1.9	7.18	0.166	0.043	0.040	0.179	2.048	0.001	0.015
475	0.78	0.017	3.7	7.98	0.369	0.090	0.048	0.228	3.498	0.001	0.003
480	1.02	0.021	4.3	8.39	0.582	0.117	0.046	0.234	2.954	0.002	0.003
485	0.95	0.002	2.3	8.20	0.264	0.065	0.058	0.237	2.526	0.002	0.003
490	1.12	0.023	3.8	8.44	0.488	0.113	0.034	0.216	2.137	0.002	0.003
495	1.03	0.003	2.2	7.98	0.243	0.061	0.036	0.189	2.356	0.001	0.003
500	1.00	0.002	2.4	7.77	0.258	0.069	0.039	0.211	2.712	0.003	0.002
505	0.97	0.002	10.1	7.88	0.261	0.074	0.065	0.224	2.220	0.001	0.002
510	0.92	0.003	2.9	7.65	0.297	0.081	0.059	0.216	2.307	0.004	0.003
515	0.96	0.158	5.3	8.28	0.617	0.140	0.070	0.277	3.073	0.002	0.003
520	0.87	0.116	7.6	8.77	0.978	0.191	0.071	0.291	4.219	0.002	0.003
525	0.83	0.004	2.6	8.16	0.211	0.046	0.052	0.184	2.201	0.003	0.003
530	1.00	0.010	2.2	7.71	0.208	0.052	0.055	0.194	2.312	0.001	0.003
535	0.99	0.006	2.3	7.74	0.224	0.057	0.046	0.181	2.058	0.004	0.003

Depth	Dry Bulk Density	C_{inorg}	Electrical conductivity	pH	Ca	Mg	Na	K	HCO_3	Cl	SO_4
cm	g/cm^3	wt. %	(mS/cm)/kg	SU	mg/kg	mg/kg	mg/kg	mg/kg	mg/kg	mg/kg	mg/kg
540	0.92	0.003	2.4	7.65	0.209	0.052	0.047	0.186	1.899	0.001	0.004
550	1.05	0.007	2.5	7.62	0.240	0.059	0.056	0.215	1.603	0.001	0.003
560	0.96	0.006	3.2	7.76	0.323	0.074	0.055	0.227	2.002	0.001	0.005

NA = Not determined

Depth	Total Extractable P	$P_{mineral}$	$P_{organic}$	P_{oxide}	P_{min}	$P_{organic}$	P_{oxide}	Opal	C_{org}	$\delta^{13}C_{org}$	C:N
cm	μmol/g	μmol/g	μmol/g	μmol/g	%	%	%	wt. %	wt. %	‰	
5	4723.9	3433.1	2598.8	1308.0	17.3	27.7	55.0	17.3	1.5	-16.1	18.2
10	5391.1	3247.0	3540.8	622.2	22.8	11.5	65.7	13.5	2.6	-16.2	25.2
15	5401.7	2129.6	3236.2	1050.1	20.6	19.4	59.9	13.2	1.3	-16.9	8.9
20	868.1	1717.5	25.5	0.0	97.1	0.0	2.9	12.8	1.4	-16.9	9.3
25	3835.6	990.8	2536.3	142.8	30.2	3.7	66.1	11.1	1.2	-17.1	9.1
30	4325.4	1162.1	2941.4	383.3	23.1	8.9	68.0	11.3	1.2	-16.4	8.6
35	4079.1	2255.2	2788.3	457.8	20.4	11.2	68.4	10.8	1.2	-16.5	13.8
40	3750.4	2351.5	2526.4	50.1	31.3	1.3	67.4	11.9	1.1	-17.6	6.8
45	3874.0	2451.8	2186.6	0.0	43.6	0.0	56.4	9.5	1.1	-17.5	10.2
50	4742.8	1968.9	2577.0	623.5	32.5	13.1	54.3	14.3	1.0	-16.4	12.7
55	2236.8	2147.2	1869.9	0.0	16.4	0.0	83.6	17.6	1.0	-17.5	7.9
60	4635.4	1795.8	2504.0	87.2	44.1	1.9	54.0	16.4	1.0	-18.2	7.4
65	5183.6	1620.7	2584.8	223.4	45.8	4.3	49.9	10.4	1.0	-16.9	7.4
70	4383.5	1507.7	1724.8	0.0	60.7	0.0	39.3	15.0	1.0	-16.5	7.2
75	5534.2	828.0	2341.4	420.7	50.1	7.6	42.3	14.6	0.9	-17.6	6.4
80	6059.7	242.6	2308.1	669.5	50.9	11.0	38.1	17.2	0.9	-17.6	7.5
85	6030.5	614.9	2460.9	732.6	47.0	12.1	40.8	24.6	0.8	-18.6	8.2
90	5466.8	1153.7	2386.5	384.8	49.3	7.0	43.7	25.3	0.9	-22.0	8.3
95	4338.9	1605.9	2199.6	0.0	49.3	0.0	50.7	21.3	1.1	-20.6	8.3
100	3406.3	1155.5	1555.8	0.0	54.3	0.0	45.7	26.6	0.6	-20.2	6.2
105	4946.7	1390.5	2602.9	195.0	43.4	3.9	52.6	19.8	1.3	-21.9	14.8
110	3694.4	1042.3	1856.6	0.0	49.7	0.0	50.3	21.7	0.5	-19.5	3.6
115	3207.3	746.2	1508.5	0.0	53.0	0.0	47.0	19.1	0.5	-20.8	6.8
120	4100.1	783.6	308.5	0.0	92.5	0.0	7.5	32.3	0.3	-19.3	2.5
125	2194.7	5914.8	0.0	0.0	100.0	0.0	0.0	37.9	0.5	-19.3	4.0
130	1976.3	1569.1	0.0	508.3	77.3	25.7	-3.0	45.4	0.3	-18.8	3.7
135	3150.0	988.2	1372.5	296.7	47.0	9.4	43.6	32.4	0.3	-19.0	3.4
140	2773.3	898.1	1282.0	185.1	47.1	6.7	46.2	19.1	0.4	-17.7	3.1
145	4157.5	1220.4	2002.0	0.0	51.8	0.0	48.2	8.6	0.9	-16.8	12.0
150	4714.4	927.6	2118.1	39.0	54.2	0.8	44.9	18.1	0.9	-17.4	9.5
155	5912.4	3222.7	2002.3	1246.5	45.1	21.1	33.9	25.0	0.6	-18.3	5.0

Depth	Total Extractable P	$P_{mineral}$	$P_{organic}$	P_{oxide}	P_{min}	$P_{organic}$	P_{oxide}	Opal	C_{org}	$\delta^{13}C_{org}$	C:N
cm	μmol/g	μmol/g	μmol/g	μmol/g	%	%	%	wt. %	wt. %	‰	
160	4459.4	1154.5	1714.6	0.0	61.6	0.0	38.4	18.6	0.6	-18.0	9.5
165	4011.7	1126.3	1400.7	0.0	65.1	0.0	34.9	24.0	0.5	-18.1	4.5
170	5151.0	1137.4	1371.2	300.0	67.6	5.8	26.6	23.5	0.4	-18.1	4.1
175	3987.3	1244.9	1321.9	39.1	65.9	1.0	33.2	22.9	0.3	-17.6	4.4
180	6305.9	1090.9	1507.0	347.1	70.6	5.5	23.9	22.1	0.3	-18.5	3.4
185	3461.7	1268.3	951.4	0.0	72.5	0.0	27.5	30.8	0.2	-17.9	3.3
190	5752.7	1064.5	741.1	0.0	87.1	0.0	12.9	39.6	0.3	-19.4	1.8
195	4802.1	1179.3	1399.2	322.5	64.1	6.7	29.1	34.9	0.2	-17.0	6.0
200	7620.6	1368.9	1065.5	0.0	86.0	0.0	14.0	36.1	0.1	-18.1	2.0
205	18091.5	2872.4	1190.1	478.9	90.8	2.6	6.6	41.1	0.5	-20.2	3.6
210	37290.9	1656.5	1053.8	207.4	96.6	0.6	2.8	44.5	0.3	-23.5	8.7
215	7750.9	2372.6	1162.3	0.0	85.0	0.0	15.0	58.9	0.4	-23.6	4.8
220	8346.2	1889.4	789.8	0.0	90.5	0.0	9.5	38.3	0.5	-21.5	8.4
225	26250.5	2762.2	1199.8	77.6	95.1	0.3	4.6	38.3	0.4	-21.7	3.3
230	18722.1	2155.9	1392.9	727.5	88.7	3.9	7.4	42.3	0.4	-21.3	4.6
235	18863.2	1757.1	1611.7	1130.9	85.5	6.0	8.5	38.8	0.2	-19.7	2.6
240	14383.5	1373.7	630.1	543.9	91.8	3.8	4.4	40.9	0.3	-19.3	1.7
245	20810.8	1932.4	1084.3	996.6	90.0	4.8	5.2	47.5	0.4	-23.3	4.0
250	13398.4	1231.9	615.8	1529.6	84.0	11.4	4.6	32.9	0.2	-19.8	2.1
255	14100.3	942.4	522.4	815.9	90.5	5.8	3.7	47.2	0.4	-19.5	1.1
260	11368.5	970.5	622.1	664.2	88.7	5.8	5.5	51.1	0.3	-19.3	1.1
265	10039.5	922.3	743.7	842.4	84.2	8.4	7.4	43.4	1.5	-18.9	1.0
270	5883.7	780.5	882.8	1567.7	58.3	26.6	15.0	49.9	0.1	-19.5	1.8
275	4548.1	934.5	899.3	401.8	71.4	8.8	19.8	58.3	0.2	-19.8	1.6
280	2769.5	995.2	639.9	0.0	76.9	0.0	23.1	55.5	0.1	-20.8	0.7
285	3758.1	1314.4	1211.7	828.9	45.7	22.1	32.2	39.8	0.2	-20.2	1.5
290	999.4	0.9908	8.6	0.0	99.1	0.0	0.9	40.8	0.2	-20.4	1.5
295	2328.5	1.1621	1166.4	0.0	49.9	0.0	50.1	35.4	0.2	-20.6	1.6
300	2435.2	2.2552	10.7	169.4	92.6	7.0	0.4	26.6	0.2	-20.3	1.6
305	4569.8	2.3515	2082.3	136.0	51.5	3.0	45.6	38.1	0.4	-19.4	1.8
310	3817.6	2.4518	1365.8	0.0	64.2	0.0	35.8	30.2	0.3	-21.3	2.0

Depth	Total Extractable P	$P_{mineral}$	$P_{organic}$	P_{oxide}	P_{min}	$P_{organic}$	P_{oxide}	Opal	C_{org}	$\delta^{13}C_{org}$	C:N
cm	μmol/g	μmol/g	μmol/g	μmol/g	%	%	%	wt. %	wt. %	‰	
315	3561.2	1.9689	1317.3	275.0	55.3	7.7	37.0	29.3	0.3	-20.2	2.6
320	4622.7	2.1472	1636.3	839.2	46.4	18.2	35.4	31.1	0.2	-21.6	5.0
325	3163.9	1.7958	1368.1	0.0	56.8	0.0	43.2	36.0	0.2	-20.3	2.0
330	3593.5	1.6207	1712.1	260.7	45.1	7.3	47.6	33.9	0.2	-18.7	1.6
335	2983.9	1.5077	1476.2	0.0	50.5	0.0	49.5	26.2	0.3	-21.5	4.0
340	1815.1	0.8280	987.2	0.0	45.6	0.0	54.4	18.9	0.3	-20.9	3.0
345	848.8	0.2426	554.0	52.2	28.6	6.1	65.3	9.5	0.2	-19.7	1.9
350	1939.1	0.6149	1324.2	0.0	31.7	0.0	68.3	25.3	0.4	-18.3	2.4
355	2844.4	1.1537	1492.2	198.4	40.6	7.0	52.5	32.0	0.4	-19.4	4.1
360	3042.9	1.6059	1242.4	194.6	52.8	6.4	40.8	31.0	0.4	-19.9	4.3
365	3264.2	1.1555	1536.8	571.9	35.4	17.5	47.1	26.4	0.4	-19.3	2.8
370	3528.8	1.3905	1829.6	308.7	39.4	8.7	51.8	25.7	0.4	-20.5	4.2
375	2411.3	1.0423	1108.5	260.5	43.2	10.8	46.0	46.9	0.3	-21.0	2.9
380	1662.5	0.7462	577.3	339.1	44.9	20.4	34.7	48.3	0.2	-20.5	2.3
385	1757.0	0.7836	948.9	24.6	44.6	1.4	54.0	45.6	0.2	NA	NA
390	7984.8	5.9148	1016.3	1053.7	74.1	13.2	12.7	30.9	0.4	-18.8	2.2
395	2704.3	1.5691	720.3	414.9	58.0	15.3	26.6	41.7	0.3	-20.2	3.2
400	2758.2	0.9882	1596.3	173.7	35.8	6.3	57.9	36.1	0.3	-18.1	2.3
405	2507.7	0.8981	1609.6	0.0	35.8	0.0	64.2	33.1	0.3	-18.0	2.0
410	2682.7	1.2204	1085.8	376.5	45.5	14.0	40.5	36.5	0.3	-18.2	2.9
415	2681.6	0.9276	1554.4	199.6	34.6	7.4	58.0	37.2	0.2	-18.0	2.0
420	4121.9	3.2227	899.2	0.0	78.2	0.0	21.8	44.8	0.2	-21.6	2.8
425	2694.2	1.1545	1478.0	61.7	42.9	2.3	54.9	51.6	0.2	-18.7	6.3
430	2059.5	1.1263	933.2	0.0	54.7	0.0	45.3	51.2	0.2	-19.1	21.7
435	2543.4	1.1374	1369.1	37.0	44.7	1.5	53.8	48.8	0.2	-18.6	1.8
440	2597.2	1.2449	1352.3	0.0	47.9	0.0	52.1	52.6	0.2	-18.9	2.5
445	2537.2	1.0909	1446.3	0.0	43.0	0.0	57.0	47.9	0.2	-19.2	3.6
450	2528.0	1.2683	1259.6	0.0	50.2	0.0	49.8	52.5	0.2	-20.4	3.1
455	2623.6	1.0645	1067.0	491.9	40.6	18.8	40.7	49.1	0.2	-20.7	2.7
460	2497.3	1.1793	1120.0	198.0	47.2	7.9	44.8	43.8	0.2	-21.1	3.3
465	2051.8	1.3689	296.8	386.1	66.7	18.8	14.5	39.3	0.2	-19.2	2.3

Depth	Total Extractable P	$P_{mineral}$	$P_{organic}$	P_{oxide}	P_{min}	$P_{organic}$	P_{oxide}	Opal	C_{org}	$\delta^{13}C_{org}$	C:N
cm	μmol/g	μmol/g	μmol/g	μmol/g	%	%	%	wt. %	wt. %	‰	
470	4386.7	2.8724	1353.6	160.6	65.5	3.7	30.9	39.8	0.2	-19.8	2.8
475	3740.3	1.6565	1897.7	186.2	44.3	5.0	50.7	23.1	0.2	-19.1	1.4
480	4160.3	2.3726	1787.8	0.0	57.0	0.0	43.0	25.7	0.3	-18.6	2.5
485	3758.2	1.8894	1868.8	0.0	50.3	0.0	49.7	14.1	0.2	-18.0	2.7
490	5478.6	2.7622	1185.8	1530.6	50.4	27.9	21.6	13.0	0.2	-19.4	2.5
495	4170.6	2.1559	1642.8	371.9	51.7	8.9	39.4	11.8	0.2	-17.8	2.1
500	3754.1	1.7571	1896.9	100.1	46.8	2.7	50.5	17.2	0.2	-18.0	1.9
505	3739.8	1.3737	1856.7	509.4	36.7	13.6	49.6	17.9	0.2	-19.0	2.5
510	3130.0	1.9324	1197.6	0.0	61.7	0.0	38.3	13.3	0.3	-18.8	2.0
515	3283.8	1.2319	1687.1	364.8	37.5	11.1	51.4	17.1	0.2	-18.7	2.6
520	3096.9	0.9424	1921.7	232.8	30.4	7.5	62.1	15.7	0.2	-18.5	2.3
525	2605.6	0.9705	1635.1	0.0	37.2	0.0	62.8	17.0	0.3	-17.7	3.6
530	2451.6	0.9223	1492.2	37.2	37.6	1.5	60.9	17.1	0.3	-19.6	5.2
535	2142.5	0.7805	1362.0	0.0	36.4	0.0	63.6	14.1	0.3	-19.3	2.6
540	2402.3	0.9345	1393.5	74.3	38.9	3.1	58.0	16.2	0.2	-18.2	NA
550	2533.9	0.9952	1462.5	76.3	39.3	3.0	57.7	15.3	0.3	-18.5	2.7
560	2272.7	1.3144	958.3	0.0	57.8	0.0	42.2	19.2	0.3	-19.3	3.2

NA = Not determined

VITA

Kristi Lynn Teter

Candidate for the Degree of

Master of Science

Thesis: PALEOENVIRONMENTAL RECONSTRUCTION OF PALEO-LAKE MABABE, NORTHWESTERN BOTSWANA FROM SEDIMENT CHEMISTRY AND BIOLOGICAL PRODUCTIVITY DATA

Major Field: Geology

Biographical:

Education: Graduated from Mustang High School in Mustang, Oklahoma in May 2002. Attended Aarhus Universitet in Aarhus, Denmark in the Spring of 2005. Received a Bachelors of Science degree in Geology from Oklahoma State University in May of 2007. Completed the requirements for the Master of Science degree in Geology at Oklahoma State University, Stillwater, Oklahoma in December, 2009.

Experience: Research Assistantship: American Association of Petroleum Geologists (AAPG) Overpressure Database Management, Boone Pickens School of Geology Teaching Assistantship (2007-2009), Geologist- Devon Energy Brazil Exploration (Aug 2009-present).

Professional Memberships: Oklahoma State University Geological Society (2007-2009), Oklahoma City Geological Society (2007-2009), American Association of Petroleum Geologist (2007-2009), Geological Society of America (2006-2009)

Name: Kristi Lynn Teter Date of Degree: December, 2009

Institution: Oklahoma State University Location: Stillwater, Oklahoma

Title of Study: PALEOENVIRONMENTAL RECONSTRUCTION OF PALEO-LAKE MABABE, NORTHWESTERN BOTSWANA FROM SEDIMENT CHEMISTRY AND BIOLOGICAL PRODUCTIVITY DATA

Pages in Study: 71 Candidate for the Degree of Master of Science

Major Field: Geology

Scope and Method of Study: Sediment samples were collected from trenches excavated in the Mababe Depression, northwestern Botswana. At present the Mababe Depression is dry Acacia parkland, but has sustained relatively large paleolakes. Sediment samples were used to determine the paleo-chemistry and paleo-productivity in Paleo-lake Mababe by determining concentrations of: soluble major cations (K, Na, Ca, Mg) and anions (Cl, SO_4, NO_3, HCO_3), P, biogenic silica, inorganic carbon, and organic carbon. The major cations and anions provide information about past lake salinity, while P concentrations provide information about sediment erosion in source watersheds. Additionally, P is a nutrient that drives lacustrine biological productivity. Biological productivity was evaluated from variations in biogenic silica, organic carbon concentrations, carbon to nitrogen ratios and the stable isotope ratio of organic carbon.

Findings and Conclusions: The sediment leachate chemistry suggest that evaporative enrichment resulted in the deposition of evaporite minerals; mainly $Ca(HO_3)_2$. The inorganic carbon and mineral P concentrations may have resulted from increasing solute load from the erosion of calcretes and evaporites from local Kalahari watersheds due to regional tectonic uplift followed by, or concurrent with increased local precipitation and fluvial incision. Lacustrine paleo-productivity is controlled by water depth and availability of P. Sediment depths between 560 cm to 260 cm show evidence of fluctuating water depths within a relatively deep lake that resulted in cyclic deposition of silts, clays and occasional sands interlayered with diatomite. Tectonic tilting of the lake basin caused overall water depth to shallow, breaking the cyclic sedimentation pattern. Organic matter accumulation in this more shallow lake increased at the expense of diatom accumulation. Variations in C:N and stable carbon isotope ratios primarily records shifts in submerged and emergent vegetation due to climate perturbations.

ADVISER'S APPROVAL: Eliot Atekwana